March 2016

# Design of a Novel Concept for Harnessing Tidal Stream Power: A Continuation

Katrina Bradley
*Worcester Polytechnic Institute*

# Design of a Novel Concept for Harnessing Tidal Stream Power: A Continuation


A Major Qualifying Project submitted to the Faculty of Worcester Polytechnic Institute

In fulfillment of the requirements for the Degree of Bachelor of Science

Submitted by:

Katrina Bradley

Authorship:

Sarah Bailey

Katrina Bradley

Andrea Chan

Nathan Curtis

Lauren Richard

Date:

25 March 2016

Project Advisor:

Brian Savilonis

# Table of Contents

# Abstract

Alternative energy is in ever growing demand, and new ways to produce it are essential to power all that needs electricity. One aspect of alternative energy that has frequently been overlooked is the race to find renewable power is tidal power. Currently, tidal turbines are inefficient and not extremely popular in the world of clean power, and this project hopes to provide some insight into a potentially more feasible and efficient design. Instead of rotating fins that are positioned horizontally to the flow of the water, our design is comprised of a fin that moves linearly with the current, similarly to an eel's dorsal fin. This project is a continuation of a previous MQP which initialized the basic design, and we worked to improve the design and make it more efficient, manufacturable, and streamlined. Our tests found that a lighter fin is necessary for the required movement, and that a crankshaft, while theoretically a more power efficient option for a drive shaft, would require custom manufacturing that is not feasible on WPI's campus.

# 1. Introduction

One of the largest problems the world faces is the ever increasing demand for energy. In 2012, the world used 5.598 * $10^8$ Tera-Joules of energy, 2.2 times more energy than it used in 1973. Since then, the demand has been rising nearly every year since 1984 (IEA, 1998). At the same time, carbon dioxide emissions have doubled (EPA, 2015), leading scientists to believe global temperatures may rise between 2°F and 11.5°F by 2100 (EPA, 2014). Of all energy generation, only 1.1% was generated from geothermal, solar, wind, tidal and other renewable environmental resources (IEA, 1998). From hydroelectric sources, it is estimated that 5.04 * $10^{19}$ Joules could be exploited annually; however only less than 18% of this is currently being harvested (UNDP, 2000).

Hydropower has long been a staple of human power generation. The water wheel was first used between 300 and 100 BCE by Roman engineers to generate power and provide

irrigation (Wikander, 1999). The water wheel became a key industrial object by the Early Medieval Ages, with more than 6,000 existing in England by 1100 CE (Friedel, 2007). Major improvements of the water wheel helped spark the Industrial Revolution by allowing for more efficient processes in factories, and the basic concept can still be seen in hydroelectric dams across the world (Thompson, 2009). Although hydropower has been an established mode of power generation for centuries, its full potential has yet to be taken advantage of by current engineering projects. The untapped power that moving water provides is enough to meet more than 7% of the world's power consumption, equal to that from current hydroelectric and nuclear power generation combined (IEA, 1998).

Much of this latent power resides in the ocean in the form of tidal currents and waves. Tidal energy is both powerful and predictable; critical characteristics for large scale power generation. Harvesting this power would allow for a dependable, renewable and clean power source for coastal communities across the world. Unfortunately, current installations are limited to only a few select locations, and few are found outside of developed countries.

When attempting to solve problems that either have a natural source or deal with nature directly, it can be beneficial to turn to natural solutions as inspiration for engineering. One of these strategies, biomimetics, copies or adapts biological systems for human purposes. Because of aquatic life's natural adaptation to living in and working with water currents for movement, fish and other marine animals can serve as inspiration for engineering designs to harvest power from the ocean. Specifically, rajiform fish, such as rays, mantas and skates, have very large, flat pectoral fins which produce thrust through long vertical oscillations. Mantas typically use this motion to continually cruise through the water, which makes them ideal candidates for bio-mimicry in designing a hydrodynamic generator. This concept was previously explored by a team from MIT, who created an actuated stingray model to develop water based robots capable of movement with minimal energy expenditure.

The goal of this project was to improve on an existing design of a device that generates electrical power from the flow of water. The device was previously a series of fins that were driven by water flowing past, which in turn drives a shaft that supplies rotational energy to a

generator that produces electricity. The project was intended to simplify the existing device, as well as to achieve more efficient conversions of power for a given flow rate of water by improving fin design and material selection. The device needs to meet several key benchmarks including:

- Operation in a totally submerged setting
- Operation in such a way that there are no undue negative effects on the local flora and fauna
- Ability for control and measurement from onboard sensors and electronics

Secondary goals included ease of creation and assembly to potentially facilitate future commercialization, as well as uniformity in materials selection and processing to ease technological and production requirements. These goals were of secondary importance due to limitations, such as operational environment, and these limitations may dictate or limit the range of options available to meet the secondary goals.

Testing was accomplished by pulling the mechanism through a standing body of water at a known rate. Performance was gauged based on ability of the fin to turn the driveshafts, turning the rotation into electrical power. The design was tested with two different shafts to allow for generalizations and correlations to be made, providing paths for larger iterations in the future.

# 2. Background

As the world's growing population emits an increasing amount of atmospheric carbon pollutants due to increased energy consumption, the average global temperature rises at an alarming rate. Developed countries have begun to turn to other forms of energy such as wind, solar, geothermal, and hydropower. However, developing countries are still dependent on the usage of fossil fuels. As technology advances, these renewable energy sources have begun to match the world's energy consumption. Hydropower has been evaluated to enhance current technologies to improve power output and efficiencies.

# 2.1 Current Energy Generation Systems

## 2.1.1 Energy demand

### 2.1.1.1 Current

#### 2.1.1.1.1 Developed vs. developing countries

Developed countries which are a part of the Organization for Economic Cooperation and Development (OECD), including America, much of Europe, Canada and Australia, currently consume energy linearly with population growth. Developing countries, however, have increasing consumption at a higher rate. In 2014, the world consumed 17.7 Terawatts from all sources of energy (IEA, 2014). Change in energy use was 8% higher in developing countries than in developed countries in 2014 (IEA, 2014). The rate is slowing down for developed countries as goals and standards have been put in place to reduce fossil fuel emissions and focus on renewable energy sources.

### 2.1.1.2 Forecast

#### 2.1.1.2.1 Demand growth

For countries who are still developing, their energy consumption is expected to rapidly increase, accounting for 65% of the world's energy consumption by 2040 (Woody, 2015). It is predicted that as developing countries grow richer and improve their economy, more money will be spent on energy-consuming services. OECD countries are expected to have a slight increase of 0.5% per year which can be accounted for by their population growth while non-OECD countries are predicted to have a 2.2% increase per year as seen in Figure 1.

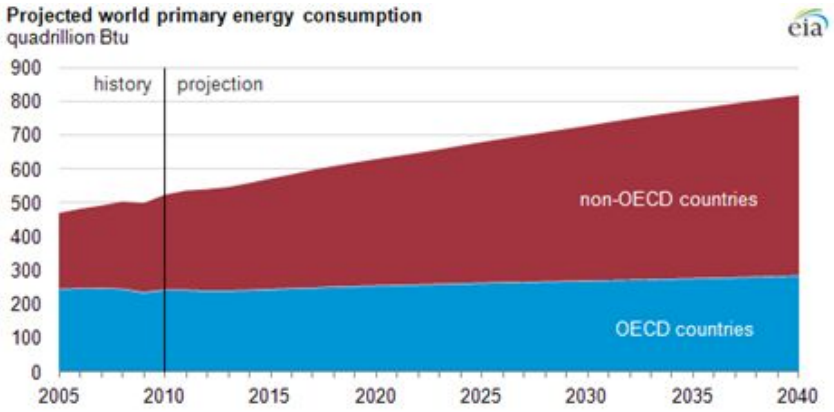


*Figure 1. Projected World Primary Energy Consumption (EIA, 2015)*

#### 2.1.1.2.2 Environmental regulations

For industrialized nations, regulations have been put in place to help reduce the carbon pollution caused by power plants. For the United States, the Clean Power Plan was enacted in 2015 to reduce carbon dioxide emissions by 32% from 2005 levels by 2030 (EPA, 2015). While developing countries have regulations and laws enacted to decrease the $CO_2$ emissions, few have been successful in reducing their carbon emissions. Some of policies have been ill-conceived with little resources provided to aid in the development of more effective environmental protection. Once in place, these regulations may lack proper enforcement, causing them to be ineffective in the reduction of fossil fuel emissions and the improvement of renewable energy sources (Issues in Science and Technology, 2015).

## 2.1.2 Need for Clean Energy

As global energy consumption increases, the greenhouse gas concentration in the atmosphere will also continue to increase. Unless the rate of carbon emissions decreases, temperatures will rise, . While the world is already starting to see the effects of global climate change, it is not too late to reduce them. By significantly decreasing the amount of $CO_2$ emitted into the atmosphere per year, the negative impact of carbon pollution can be stabilized and eventually reversed (EPA, 2015). Many other energy sources produce a minimal amount of $CO_2$

compared to fossil fuels as seen in Figure 2 ( WNA, 2011). With the use of renewable energy sources, the world can eliminate harmful fossil fuels and instead rely on energy sources that do not have a detrimental impact on the environment.

| Technology | Mean | Low | High |
|---|---|---|---|
| | tonnes $CO_2e$/GWh | | |
| Lignite | **1,054** | 790 | 1,372 |
| Coal | **888** | 756 | 1,310 |
| Oil | **733** | 547 | 935 |
| Natural Gas | **499** | 362 | 891 |
| Solar PV | **85** | 13 | 731 |
| Biomass | **45** | 10 | 101 |
| Nuclear | **29** | 2 | 130 |
| Hydroelectric | **26** | 2 | 237 |
| Wind | **26** | 6 | 124 |

*Figure 2: Energy Sources and their Carbon Footprint*

## 2.1.3 Renewable sources

### 2.1.3.1 Solar, wind

The most common renewable energy sources are solar power and wind power as they are readily available and produce very few greenhouse gases. Solar and wind farms are also the most developed technology when compared to other current renewable energy forms. In the US alone, wind energy has enough potential to produce about 10 times the country's power needs (Clean Line Energy). Both wind energy and solar energy have also become more cost-effective in recent years and are expected to decrease in price in the near future. However, both sources of power

require certain climates and geographical areas to be efficient. There must be a sufficient amount of either sunshine or wind for adequate performance of these devices (Prono, 2012).

#### 2.1.3.2 Geothermal

Another solution to reducing the dependence on fossil fuels is tapping into geothermal energy. Available almost everywhere on the planet, geothermal energy works by using hydrothermal convection systems. Cold water seeps into the Earth's crust, heats up, and rises back to the surface. The hot water is captured as steam and used to drive electric generators. Thus far, 68 billion kilowatt-hours of electricity have been produced (UCS, 2015). With a few power plants however, some air pollutants have been released into the atmosphere. Further research and development is required to improve the geothermal energy harvesting systems.

#### 2.1.3.3 Hydropower

Unlike other renewable energy forms, hydropower is one of the most mature renewable energy sources available currently. It has been used since Ancient Greece and had an increase in popularity during the Industrial Revolution. With current technologies, hydropower has improved greatly to become more efficient and cost-effective. There are now many different forms available including the use of tidal power, reservoirs, and rivers. While hydropower has some disadvantages, overall it is essential to the effort to reduce global carbon emissions (Irena, 2012).

## 2.2 Hydropower

### 2.2.1 Turbine power

In 2013, hydropower produced almost 9% of all electricity generated in the United States. Hydropower is broadly defined as power generated from kinetic energy stored in moving water. Typically, this energy is harvested through a turbine, which is embedded in a dam. A properly designed and located dam can generate a megawatt per quarter acre (EPA, 2015), an energy to

area ratio more than 20 times better than modern industrial solar installation accomplishments (UCS, 2015). Hydropower also has far lower lifetime emissions than any other industrial sources, producing 46 to 360 times less carbon dioxide equivalent per kilowatt hour compared to a coal-fired power plant (UCS, 2015). These dams are not without drawbacks, however. Dams can have devastating impacts on wildlife, both up and downstream of the dam (UCS, 2015). Upstream, dams inherently flood areas, rendering them uninhabitable for many of its former residents. Downstream, the area may experience greatly changed water flows, especially since dams are designed for constant power generation, as opposed to matching seasonal water flows. This can drastically change the habitats and ecology of land below the dam.

The other major form of hydropower is called hydrokinetic generation. This is characterized by machinery that collects power from moving water without a dam that are typically installed offshore in coastal areas. Current systems include devices that travel vertically with wave motion, pressurizing a gas that is used to produce energy. Another device is a floating reservoir which is filled with breaking waves that drive a turbine (UCS, 2015). Other hydrokinetic systems are powered by currents, using the flow of water to spin a turbine or propeller system. These various forms of hydropower produce different amounts of power as seen in Figure 3 which allows for a wide range of application depending on the power required (NCI, 2009).

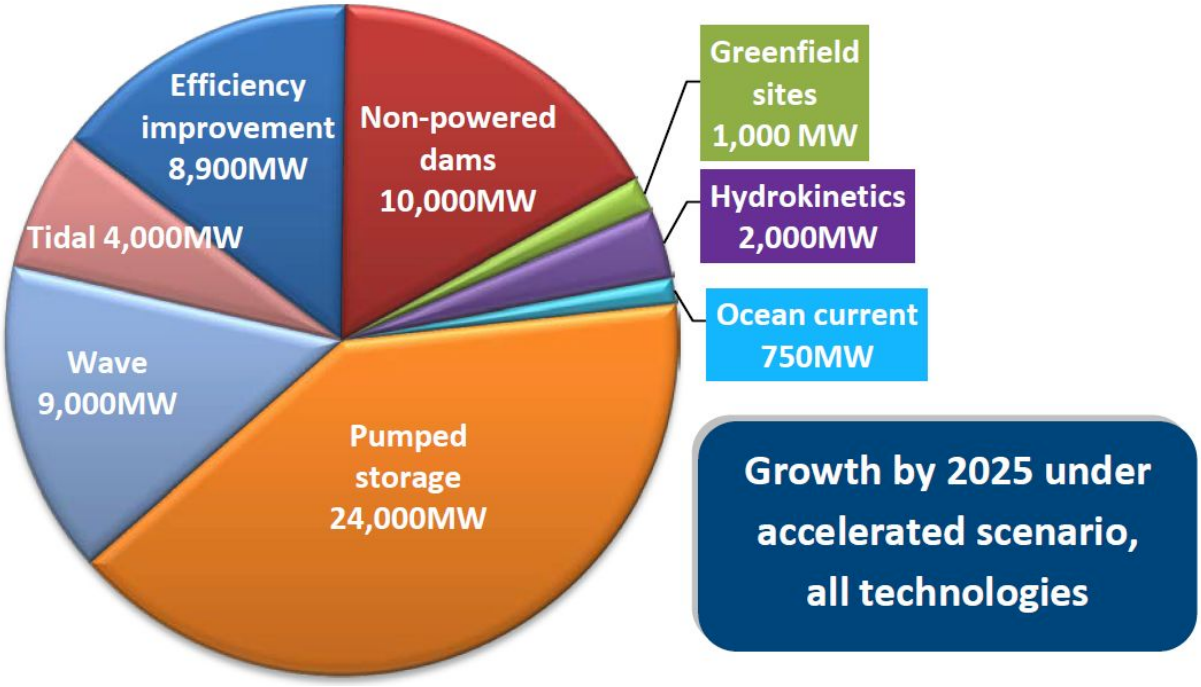


*Figure 3: Power Collected from Various Sources*

Current kinetic energy generation systems are currently less cost effective than most other forms of power generation. Hydrokinetic generation is roughly twice as expensive per kilowatt hour generated as wind energy (USC, 2015). However, proposals of new projects estimate the costs to be comparable to wind generation, which itself has become 3 to 4 times more cost effective than at its introduction. The levelized cost of energy in dollars per kilowatt hour for varying types of energy generation can be seen in Figure 4 below (GEG, 2015). Installations are also vulnerable to environmental impacts, such as corrosion or interference from the various lifeforms living in the ocean. The next generation of hydrokinetic generators should therefore be thoroughly designed to withstand the harsh environment of the ocean while simultaneously being gentle enough to avoid damaging both the generator and the environment around it.

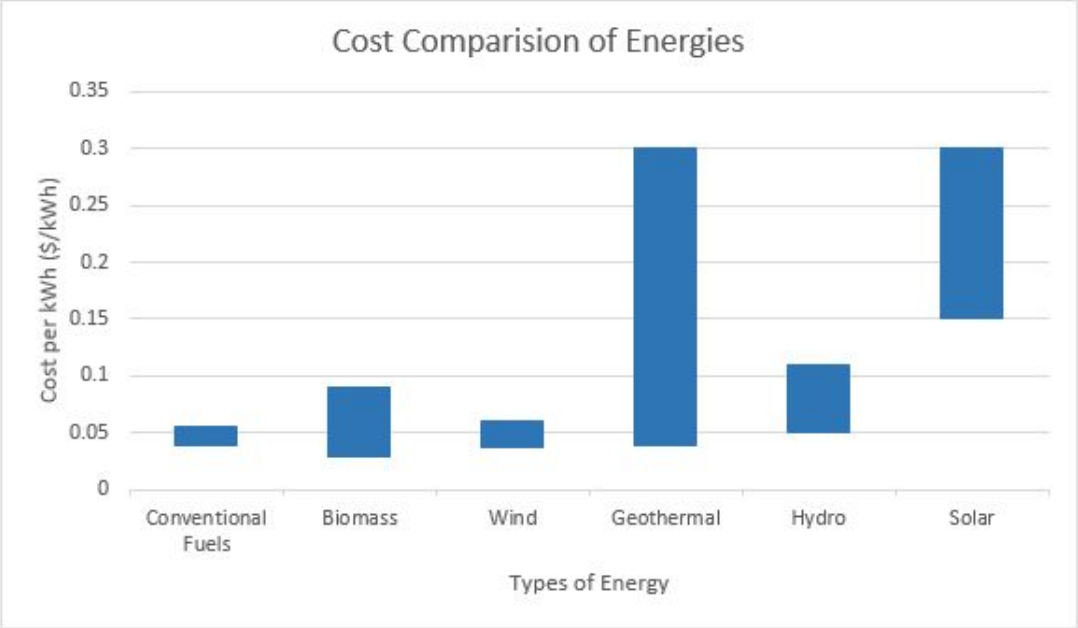


*Figure 4. Cost Comparison of Energies*

## 2.2.2 Previous Hydropower Designs

Hydropower has been harvested from sources such as tidal currents and shore waves. The Engineering Business Ltd. has been developing a submerged airfoil-like oscillator. As tidal currents flow over the foil, the device oscillates vertically to pump hydraulic cylinders and drive a hydraulic generator (DTI, 2001). A program logic control (PLC) tracks the system's parameters, including inflow velocity and arm position, to calculate the optimum angle of attack for that instant (DTI, 2003). A major limitation is the energy spent on actuating the hydraulic cylinders to dynamically change the foil's angle of attack (DTI, 2005). The estimated output capacity was 150kW.

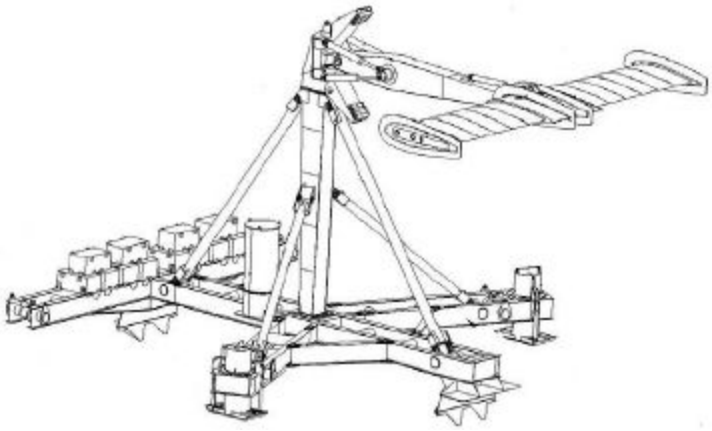

*Figure 5: .Engineering Business Ltd Model*

Under TidGen, a series of cross-flow turbines has been under development. The device captures shallow tidal currents at depths of 50 to 100 feet below the water surface. As current flows against the series of helical turbine blades, the turbine rotates and drives a shaft to the generator. The expected peak outputs are 180kW. One limitation of this design is the lack of yaw, restricting the device to capturing flow along an axis. Because a transmission line will connect directly to the generator, the design must also be robust, being capable of withstanding the pressures at installation depths while being waterproof.

*Figure 6. TidGen Model*

## 2.3. Biomimicry and Biological Systems

Biomimicry is the process of copying or adapting something found in nature to address human needs. This has been used successfully in the past to create ubiquitous systems such as Velcro and self-healing materials. This project focused on changing fish locomotion to power production, effectively reversing the natural process

### 2.3.1 Fluid dynamics of fish

Through years of evolution fish have evolved into thousands of different species. These species have evolved to have a large variety of fin designs for locomotion. Many of these fish have high-performance locomotive properties. It is these properties that make fish ideal subjects of study for both underwater vehicles and underwater energy harvesting devices. One common characteristic of all fish propulsive systems is that they use multiple control surfaces to swim by producing thrust and balancing torques (Lauder and Drucker, 2004). These control surfaces have three main groups: paired fins, median fins, and the body of the fish itself (Blevins and Lauder, 2012). Paired fins commonly consist of pectoral and pelvic fins. There are commonly three types of median fins: the dorsal, anal, and caudal fin (Lauder and Drucker, 2004). A fish can have more or fewer fins depending on the adaptations of the fish and the environment that it is living in. However, for all fish, there exists a body wave that travels along the body of the fish opposite the direction of the fish's movement (Xuelei et al, 2014). This body wave is what allows the fish to propel itself. Although there are many different modes of swimming in fish, this paper will focus on the rajiform and the anguilliform models

#### 2.3.1.1 Rajiform models

Rajiform motion is common in rayfish. This motion uses paired fins for propulsion, as opposed to using whole body motion, and has two common modes (Boileau, 2002). The first mode is oscillatory motion, where the pectoral fins oscillate, propelling the fish. Oscillatory

motion is similar to a bird flapping its wings as it flies (Rosenberger, 2001). With less than half of a full wave of the fin, the fish is able to move its fins from its lowest to its highest points. Manta, eagle, and bat rays all use this type of motion. The second mode is undulatory motion, which is defined by undulation in the pectoral fins where the fins have more than one wave present at a time. Skates and most stingrays use this form of motion for propulsion (Boileau, 2002). Between these two modes, there are large variations in fin-beat frequency, fin amplitude, and the degree of undulation. Undulation motion has a high fin beat frequency and low amplitude. This allows for high maneuverability, quick turning and moving at slow velocities. Oscillatory motion has a lower frequency and a higher amplitude, and generates lift (Boileau, 2002).

#### 2.3.1.2 Anguilliform models

Anguilliform motion is common in long bodied-forms of fish such as eels and lamprey (Vorus and Taravella, 2011). Anguilliform fish use lateral body undulations of their elongated and flexible bodies to swim, using their bodies to propel themselves as opposed to using fins. Anguilliform motion allows the fish to maneuver easily and gives them a unique backwards motion pattern (Boileau, 2002). The undulation amplitudes increase from snout to tail-tip in forward motion (Herral, et al, 2011). The opposite is true for backwards motion. The undulation frequency increases with swimming speed in both forward and reverse motions, with undulation frequency in reverse motions greater than forward motion. The amplitude and wavelength of undulation differ significantly for forward and backwards motion. The undulation frequency is related to swimming speed, however tail tip amplitude, wavelength, and stride length are not (Herral, et al, 2011).

### 2.3.2 Energy generation

Most previous research on biomimetic fins has been focused on driving the fins through an electric source, whereas this project seeks to accomplish the reverse. However, the previous research indicates that electricity to mechanical conversion is possible, so the reverse should be

possible as well. Of these studies, one reported typical efficiencies of electrical power to locomotive power between 0.08% and 0.153% (Epstein et al, 2006). While these are very low efficiencies, this study was focused entirely on generating motion and largely ignored efficiencies in conversion. Since this project looks to take conversion efficiencies into account, it can be reasonably expected to see much higher efficiencies. This project was a robot that was mimetic of a stingray, whereas ours is mimetic of an eel. The previous MQP this is based on achieved 20% efficiencies in certain circumstances, indicating that this may be a highly promising path to future power generation (Costanzo et. al, 2015). We intend on improving on the previous project, so we expect to see less internal losses, and thus a higher total efficiency.

## 2.4. Previous paper

A previous Major Qualifying Project, titled *Design of a Novel Concept for Harnessing Tidal Stream Power,* is the basis of this current project, in which the previous project team designed and manufactured a prototype of the water energy harvester that the current group plans to improve upon. The previous design consisted of a sinusoidal fin made out of neoprene and acrylic with a length of 76.2 cm. The fin drove a camshaft which converted mechanical motion into electrical power via shaft rotation.

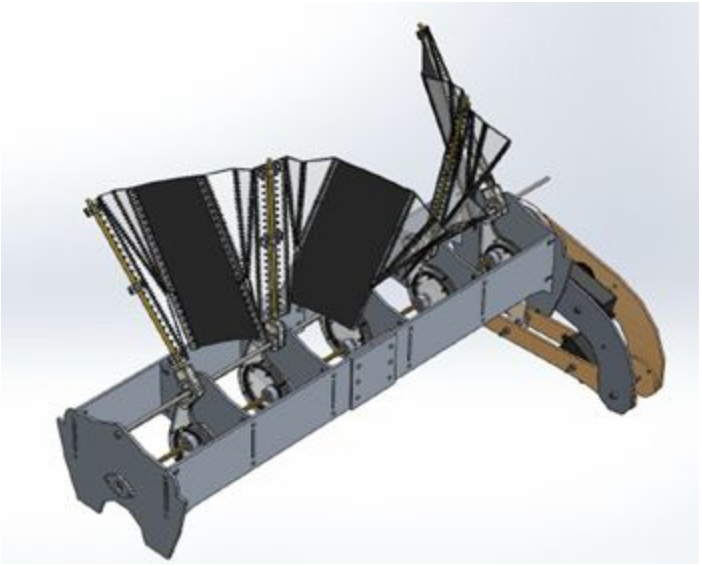

*Figure 7: CAD Model of Previous Project*

## 2.4.1 Successful aspects

### 2.4.1.1 Functioning prototype

The previous project group was successful in building a functional model that effectively produced power in a test setting. Some aspects of their design could have been improved upon, but the prototype did produce repeatable results, with the hybrid acrylic-neoprene fin producing 35 RPM at a flow speed of 1230 mm/s. This translated to roughly 5.5 N*m of torque and 2.8 Watts of power. Originally, the design called for neoprene due to its desirable material characteristics; however it was found that a hybrid fin of neoprene and acrylic had greater stiffness and was less prone to folding.

### 2.4.1.2 Mathematical basis

In order to determine the geometry of the fin, the previous group calculated that the flattened form of the sinusoid would produce an arc with a width that was equal to the height of the fin. In every case, the bottom edge of the fin exists at the axis of rotation, so the bottom segment of the fin, when pulled straight, would become the axis of rotation. The geometry is

dependent on the change of angle between cams, the length of the fin, and the radius from the center axis of the top and bottom edges of the fin. Constraints included: the size of the frame, the depth of the testing environment, and the phase of the cams.

## 2.4.2 Limitations

### 2.4.2.1 Limited testing

Due to testing limitations, there were many constraints put on not only the design of the model, but also the type of testing available for use. The first major limitation was the absence of a proper water flow tank on university property. Because of this, the previous group tested their model in the rowing tanks in the athletic facility. Significant drawbacks to this were the inability to control and accurately measure the flow rate in the tank, and restrictions in the depth of the tank which was relatively small (about 35.6 cm). This significantly constrained the design and testing of the prototype.

Another testing constraint that arose was the lack of an inexpensive dynamometer that was sensitive enough to measure the small torques produced by the fin. To remedy this, the project group designed and manufactured their own mechanical friction brake dynamometer, which consisted of two Vernier sensors: a rotation sensor to measure shaft speed and a linear force sensor that would measure the force applied tangent to the shaft.

### 2.4.2.2 Design Flaws

While designing their own prototype, the current project group wanted to address some design flaws with the original model. The first of these flaws was the design of the hybrid fin. While the fin was in motion, the acrylic tended to restrict the smoothness of motion of the fin, which would result in a less efficient model than a similar fin made of a single material designed to not lock up. Not only this, but assembling the acrylic and neoprene together was extremely time-consuming, as they were hand sewn together, and increased the possibility of ripping in the neoprene.

The second design flaw rested in the design of the shaft. While the cam shaft theoretically would be efficient at converting the sinusoidal motion into rotational motion of the shaft, there was a significant dwell apparent in the linkage that caused the system to partially lock. This made it difficult to continue to turn the shaft. While it was not as much of a problem for a model of this size, if the project were ever to be scaled up to a working life-sized prototype, this would potentially cause tremendous loss of power and efficiency.

## 2.5. Summary

Hydropower is becoming increasingly relevant as the need for alternative energy increases. Harvesting tidal energy would significantly increase the amount of energy captured each year through renewable energy harvesting devices. While there are currently many different ways to harvest tidal energy, the search for more efficient methods with fewer environmental impacts continues to be the goal for many researchers and engineers. One novel way to design new tidal energy harvesting devices is through the use of biomimicry, imitation of nature to create designs that suit human need. Through analyzing how fish move through water, this project will focus on designing a new way of harvesting power from water, continuing off of a previous project group's work. This device will mimic the natural motion of fins in order to more efficiently convert tidal waves into electrical power.

# 3. Methodology

## 3.1 Improvements

Based on the operation and test results of the old energy harvester, areas of improvement include the fin structure, drivetrain, fin to crank linkage, and torque-reduction gearing.

### 3.1.1 Fin design

The previous device had two major iterations of fin design. For the first fin, a single neoprene sheet was simply mounted to five radial posts that attached to a rocker arm. The hybrid fin structure featured a series of interconnected acrylic plates and neoprene sheets. The hybrid fin had a similar mounting scheme as the original neoprene sheet (See Figure 8). Given the flexibility of the neoprene fin and the lack of support structure, the first fin design was prone to folding under load. However, the flexibility also allowed the mechanism to capture volumetric flow similar to the fins of a fish. In contrast, the composite fin was much less flexible than the first fin. The acrylic plates are limited to hinging about the threaded joints between each other and the neoprene sheets. This restricted movement may explain why the cams had a dwell point, a topic of later discussion. The acrylic plates were also prone to folding in upon themselves, causing the neoprene to awkwardly bend in places.

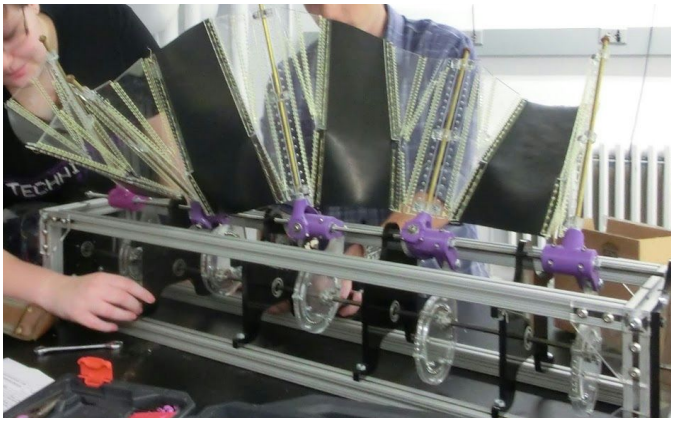

*Figure 8: Hybrid Fin Design*

When improving the fin design, the device length was kept at 76.2 cm while the number of posts increased from five to seven. Altering the number of posts changed the frequency of the fin and allows the relationship between the torque-RPM and frequency to be observed by comparing our data to that of the previous team. The transmission angle of 90 degrees was also kept the same in order to compare the effects of changing frequency between designs.

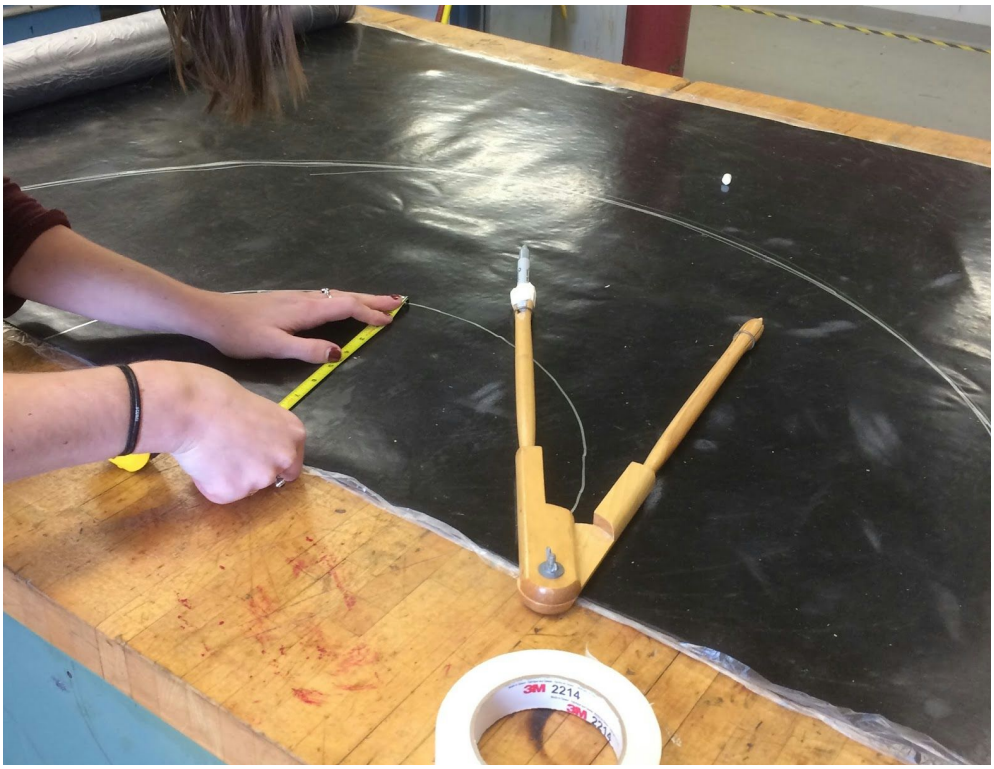


*Figure 9: Cutting the Fin*

The new design used a continuous neoprene sheet much like the first iteration of the previous group's design (Figure 9). However, instead of only using one sheet, the new design uses two sheets of ⅛" neoprene which were glued together with the mounting rods and acrylic supports in between the two sheets. The supports, which are 1" by 12" rods of acrylic that have been sanded down, prevented the fin from folding over when held upright. Since assembly was another concern for the fin design, the updated fin simplified the construction as it no longer needed the threaded joints of the hybrid fin. Eliminating the acrylic plating then improved the manufacturability as fewer complex parts and assembly were necessary. The edges of the neoprene sheets were also sewn together in order to prevent peeling of the adhesive used under pressure (Figure 10). During manufacturing on a larger scale, this could be avoided by using an industrial strength adhesive.

*Figure 10: Sewn Edges*

### 3.1.2 Drivetrain

Another significant area for design improvement was the drivetrain. With the hybrid design camshaft, there were dwells or lock points at certain points of rotation. Part of this was attributed to the cam design itself, and part of it was due to the fin. Because the acrylic plates could only move about the thread joints and were inherently inflexible, a lock point was encountered if one cam lagged behind the other four cams. It overcame the dwell only after sufficient force was applied.

To examine how output electrical power to input fluid power changes due to drivetrain design, a redesigned camshaft system and a new crankshaft system were implemented. The camshaft follows the same basic principle as the old design where a rocker attached to the fin oscillates to push and pull a cam assembly. The cam assembly's motion forces a rotation of an inner disk. Attached to the disk is a driveshaft rotating in place. The new camshaft design reevaluates the linkage system by altering the rocker arm, crank arm, and linkage arm lengths to reduce the possibility of stop points. A significant change between the old and new cam assemblies is the size of the crank disk. The crankshaft is a new design exploring how friction affects the electrical power output to fluid power input efficiency. By reducing the total number of moving parts (i.e. eliminating steel ball bearings), the crankshaft is only affected by friction between the rotating journals and their adjacent webs. Energy from the same rocker system as that of the cam is transferred through a rocker stick connected to evenly spaced journals across the crankshaft. The combined x-y force causes rotation of the journal and subsequently the entire crankshaft. Like the camshaft, the design of the crankshaft was developed using the same rocker-crank linkage path. For easy interchangeability, the crankshaft is spaced such that each journal matched up to the corresponding rocker positioned by the camshaft. The crankshaft output is a shorter driveshaft mounted at the end of the system. The entire system, including the end of the crankshaft, rotates; therefore a continuous driveshaft is not needed.

### 3.1.3 Other Considerations

A separate electrical group focused on the generation and transmission of electrical power, the sensors, nacelle, and device mounting. Both mechanical and electrical teams collaborated on gearing to step-down driveshaft speeds between the drivetrain and the induction motor. This will ensure an efficient transmission of mechanical to electrical power.

To account for potential mismatching between the mechanical system's driveshaft and the motor, an Oldham coupling connects the two shafts. Any misalignment is offset by shifting the coupling hubs a fraction of an inch. The two systems are also connected by the frame. While the drivetrain has its own system of mounting to the frame, the nacelle uses a similar method of latching into the 80/20 frame slots at the end of the frame. Unlike the acrylic pieces of the camshaft and crankshaft, the electrical system requires additional protection from water. It is enclosed in fiberglass nacelle supported by an acrylic dome-like frame. The nacelle is offset towards the top of the frame when inverted. This is to both prevent water from entering the nacelle and to properly connect to the driveshaft. Sensors inside the nacelle deliver critical data about the surrounding environment such as flow direction and speed, nacelle temperature, and internal moisture levels.

## 3.2 Component Design

### 3.2.1 Fin

#### 3.2.1.1 Fin Shape

The design of the fin was similar to the previous group's design. The overall length of the fin was chosen to be as close to the previous design to make comparisons between the old fin designs and the new fin designs. With a similar length, there was only a small increase in surface area, due to a slightly differing width, therefore the volume of water running over the fin has changed by an inconsequential amount. The number of masts and thus the sinusoidal wavelength

created by the fin also increased because of this. The fin was designed to create one and a half periods of a sine wave along its length to increase the frequency of the sinusoid and improve power delivery to the drivetrains. Mathcad was used to determine the dimensions of the design for the final calculations; this can be found in Appendix A. The planar geometry of the fin is an arc section, where the top and bottom edges define the curvature of the wave formed. The fin dimensions include a bottom arc length of 0.77 m and a top arc length of 1.73 m with a radius of 0.30 m between the two arcs. There are seven 0.30 cm masts placed equidistant from each other along the fin.

The geometry of the fin is a function of the angular position of the masts, the total length of the fin, the radius from the center axis to the top of the fin, and the radius from the center axis to the bottom of the fin (Costanzo et. al, 2015). Both the length and radius of the fin were constrained based on the testing environment and chosen to match that of the previous model. As in the previous model, the peak-to-peak amplitude of the fin was chosen to be 90 degrees so that the transmission angles at the joint where the rocker connects to either the cam or the crankshaft linkage will be 45 degrees. This angle is a generally understood maximum for transmission angles. The planar geometry of the fin was calculated using the following equations:

$$\lambda = \frac{2\pi d}{\phi n} \tag{1}$$

$$form(x) = \theta max * sin(2\pi \frac{x}{\lambda}) \tag{2}$$

$$edgeL(r) = \int_0^{len} \sqrt{1 + [\frac{d}{dl}((form(l) * r))]^2}\, dl \tag{3}$$

Equation (1) gives the wavelength of the fin ($\lambda$), where d is the distance between masts, $\phi$ is the angular position of the masts, and n is the number of masts in a single wavelength. Equation (2) gives the angular displacement from vertical of the fin along its length (form(x)). $\theta max$ represents the maximum angular displacement of the fin from vertical and $x$ is the distance along the fin. Equation (3) represents the arc length along the fin, where $len$ is the total length, in this case 76.2 cm, and r is the radius. Equation (3) was used to determine the length

along the top and bottom arc of the fin. The final planar fin geometry can be seen in Figure 11. Once the planar model had been calculated, a three-dimensional model was then designed in SolidWorks.

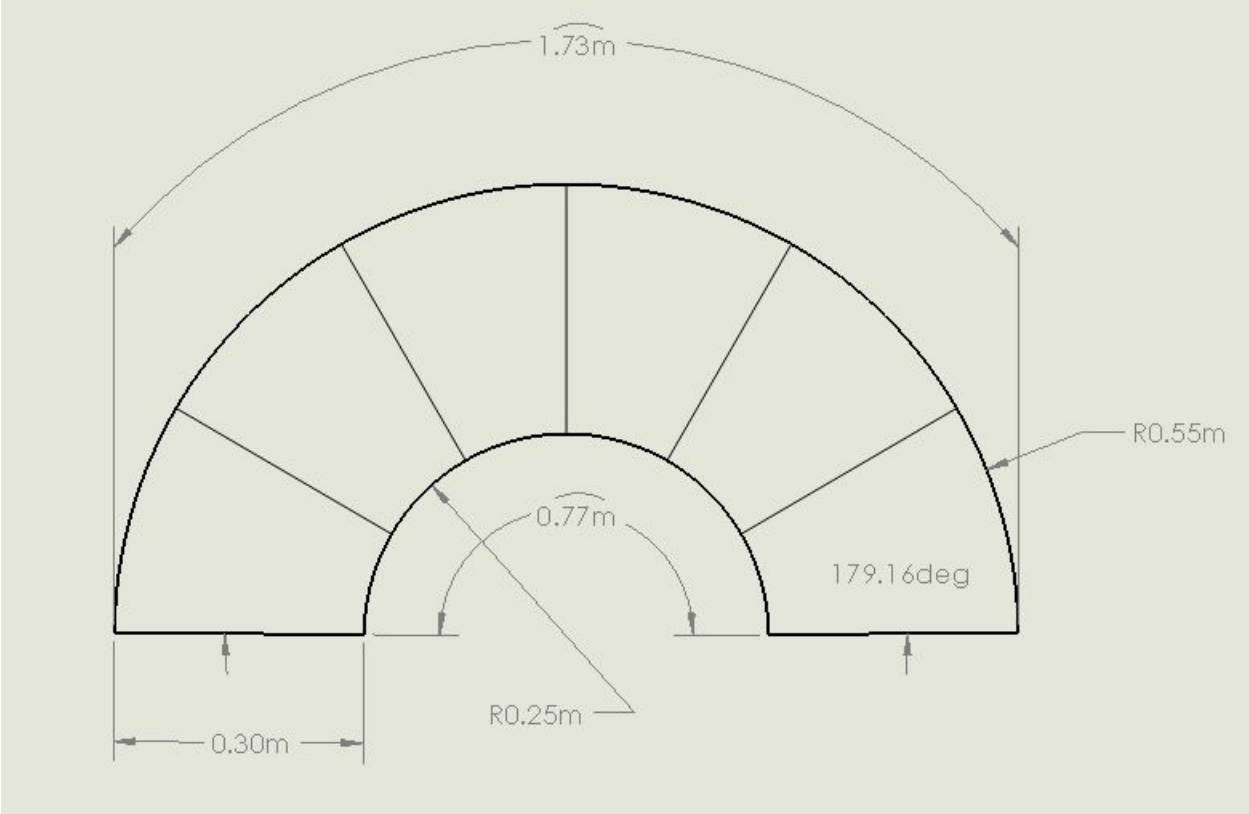


*Figure 11: Planar Fin Geometry*

*Figure 12: SolidWorks Model of Fin with Masts*

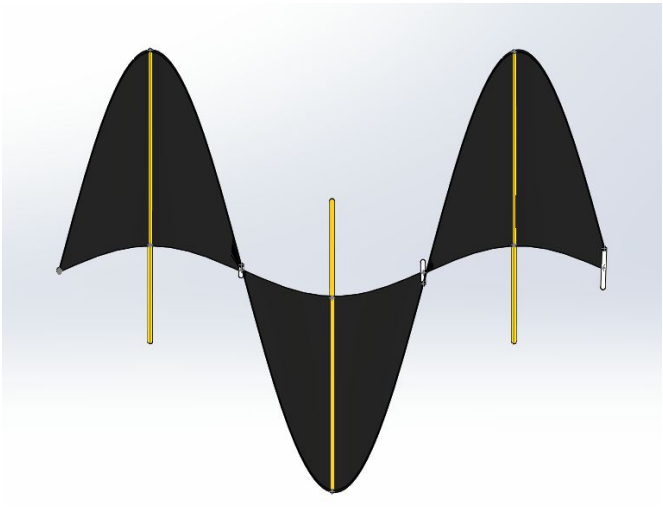

*Figure 13: Top View of SolidWorks Model of Fin with Masts*

### 3.2.2.1 Linkage System

The cam and crankshafts were both designed using the same linkage system. This was done to ensure the interchangeability of the drivetrains. The linkage system was designed to be a

four-bar crank-rocker linkage using the Linkages Software by Norton. Once the linkage was designed, it was created in Solidworks as a skeleton design for the cam and crankshafts. The rocker motion was set at 90 degrees to create 45 degree transmission angles, which is the maximum acceptable transmission angle for a linkage system (Norton, 2012). The linkage system designed is shown in Figure XX, the dimensions for this design can be seen in the Figure 9. In this design, the rocker drives the crank, which is different from how a crank rocker linkage usually works, where the crank would drive the rocker. In an energy generation system, the masts move with the fin through a flow of water; driving the cam or crankshaft, which in turn rotates the driveshaft which is connected to the motor. The mast connects to linkage system on linkage four. Linkage four is an elbow shape and the mast is press fit into this linkage and held with adhesive.

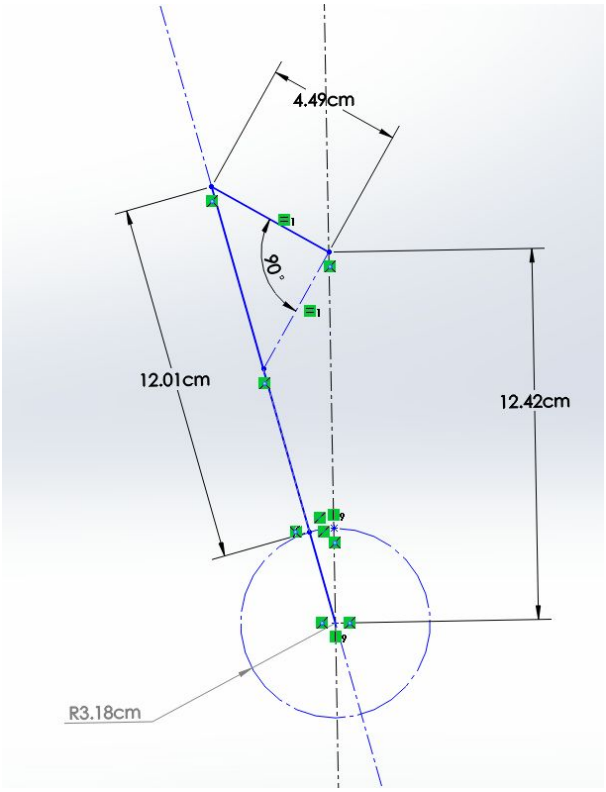


*Figure 14:. Schematic of Linkage System*

#### 3.2.2.2 Camshaft

The camshaft design from the previous MQP suffered from frictional losses and dwell points. The ball bearings frequently got caught on the cam slots, leading to excess friction within the system. Another problem was that the cam would often get stuck when rotating, leading to a loss of power transmission. There could be several reasons for this, such as a dwell in the cam or a flaw in the dimensioning.

Dynacam Software was used to design the inner cam to produce the 90 degrees needed to create the sine wave in the fin. After the inner cam dimensions had been determined, a Solidworks model was created for this inner circle. Once the inner cam was designed, it allowed for a design for the outer piece of the cam so that the shape matched the dimensions of the four-bar linkage. This new design should have no dwell in the cam motion, and the ball bearings fit together with minimal space between each ball. The dimensions to the cam were changed to allow for the cam and crank shafts to be interchangeable.

The eccentric cam converted rotational motion into reciprocating motion. The ribbon fin then transferred rocker motion through a cam that spins an output shaft. The output shaft is a single solid rod that runs through all of the cams. Ball bearings with 0.6 cm diameter were purchased and placed in channels cut into the cams. Ball bearings were used to decrease frictional forces, however there is still friction between the ball bearings and the acrylic with a coefficient of friction of approximately 0.4-0.5$\mu_s$. Graphite lubricant was used to decrease this coefficient. Three layers of 0.32 cm thick acrylic will be bolted together for the outer ring leaving slots for 0.6 cm steel balls to act as the ball bearing assembly. A rocker assembly connects the masts of the fin to the crank. The base of the mast is fixtured to the rocker linkage. This rocker assembly allows for a 90 degree rocker motion of the masts, that is 45 degrees from vertical each way. The rocker drives the crank causing both the inner ring and the driveshaft to rotate 360 degrees. As the driveshaft rotates, the torque, theoretically, would be translated into power using the motor.

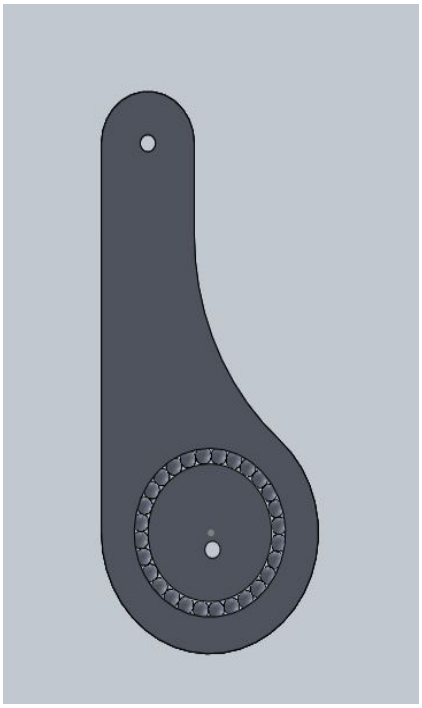

*Figure 15: Single Cam in SolidWorks*

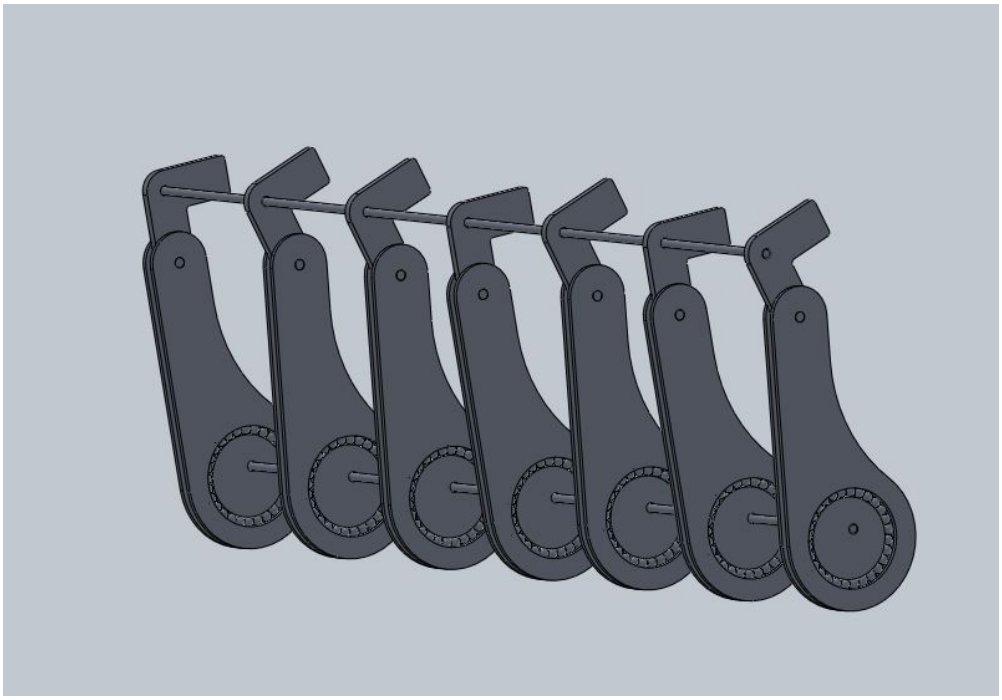

*Figure 16: Camshaft Assembly in SolidWorks*

### 3.2.2.3 Crankshaft

Linear reciprocating motion from the fin was converted into rotational motion to a driveshaft via a crankshaft. A crankshaft consists of journals and webs that act as a central drivetrain would. The new design is modular, with separately machined webs, journals, and driveshaft spacers made out of acrylic. The webs and spacer journals are connected using acrylic adhesive and a bolt, preventing the journals from rotating around the flat edge of the webs. On the other side, the true journal was also attached using acrylic adhesive and a bolt, but is cylindrical in shape and has a spinning collar attachment which allowed for connection to the rockers. As force from the rocker linkage was applied to a journal, the journal and web rotated and thus transferred torque to the motor attached in the nacelle. The staggered journals ensured that for each crank distributed across various angles along the shaft, all positions of the fin can be accounted for in delivering power.

The total effective length of the crankshaft was the same as the total length of the masts, 76.2 cm. The actual shaft length is slightly greater than 76.2 cm to allow for mounting to the frame and attachment to the gearbox. The diameter of the journals was 2.54 cm. Given acrylic's shear strength of 55 MPa, this will ensure the driveshaft will be able to withstand the load torque of the water. To prevent interference with the fins and mast, the length between the center shaft and the journal connection was calculated to be 6.4 cm. A hole with depth 0.89 cm was used for the rocker-journal connection. The rocker connects to the journal with a pin that runs through the face of the journal and its connecting webs at said depth. An early iteration crankshaft is pictured below in Figure 17, but the final design included journals which were rectangular in shape in order to simplify the machining process.

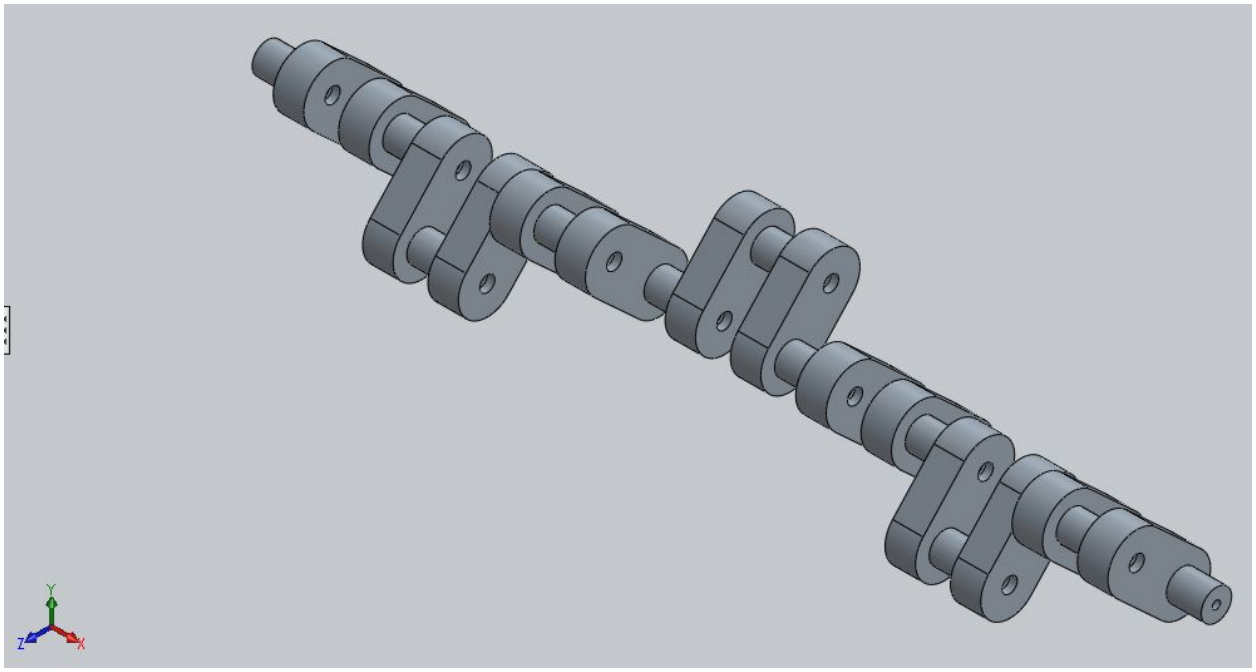

*Figure 17: SolidWorks Diagram of the Crankshaft*

The crankshaft was mounted in a similar fashion as the camshaft. Bearings supported the ends and central parts of the crankshaft, enabling free rotation in relation to the frame. A gear was attached to the end of the driveshaft to transfer shaft power into the gearbox.

### 3.2.2.4 Gearbox

The direct output from the fin was designed to be low velocity with high torque mechanical power. To effectively convert this power into electrical energy, the output must be reduced into high velocity, low torque power. A gearbox connected between the driveshaft and the induction motor shaft to properly reduce the power.

From the previous energy harvester, the maximum shaft speed was observed to be 35 RPM for the hybrid fin while it was 25 RPM for its 30.5 cm neoprene counterpart. The maximum observed torque was 3 N*m and 3.6 N*m respectively. The minimum speeds were 1.5 RPM and 1 PRM. Using the fundamental laws of gearing, the gear ratio may be calculated (Norton, 2012).

*Table 1. Fundamental Laws of Gearing*

| | | |
|---|---|---|
| | $m_V = km_T$ | (4) |
| | $m_V = \frac{\omega_{in}}{\omega_{out}} = \pm\frac{r_{in}}{r_{out}} = \pm\frac{d_{in}}{d_{out}}$ | (5) |

The driving parameter is the expected range of speeds at which the motor will generate electricity. This value was determined by the electrical group to be at least 1000 RPM for their chosen motor. This determined the ratio to be in the area of 60:1, a very difficult gearing ratio to accomplish with the losses that will happen in the gearbox.

## 3.2.3 Frame

The 8” x 7” x 38” frame was composed of twelve connected pieces of 80/20 aluminum bars connected with acrylic corner plates. This frame was salvaged from the previous MQP to save time building the overall mechanism and because 80/20 could be easily modified to add external supports. To hold the camshaft and crankshaft drivetrains in the frames, several acrylic

support plates are placed across the frame. Both the rocker shaft and the driveshaft have individual acrylic supports to help distribute the weight. These supports use two glued pieces of 1/8” acrylic to reduce the likelihood of deflection. Embedded into the glued acrylic is a single ¾” inner diameter bearing that allows the shafts to spin freely in the support. At the ends of each support plate, there are keys that allow the plates to slide into the 80/20 bars. To ensure the cam and crank follow the correct linkage paths, the support plate bearing holes are offset to be slightly above the upper limit of the frame.

# 3.3 Material Selection

## 3.3.1 Materials and Cost Analysis

When selecting the proper materials for construction, the cost was a big consideration. However, a balance was struck between material properties necessary for proper functionality and the cost of material. This was due to the fact that various components of the design required different materials because they each have different tasks. The camshaft, the crankshaft, the fin, and the driveshaft were the main consideration for this section. For the camshaft, laser-cut acrylic was chosen as it would provide a durable material at a low cost. A 61 x 122 x 0.32 cm sheet of strengthened, UV-resistant acrylic sheet costs approximately $40. This acrylic has excellent tensile strength of 8,000-11,250 psi at a temperature range of 32F to 170F. These properties all fall within necessary tolerances based on expected forces, as seen below in the Ansys simulation. For the crankshaft, acrylic rectangular rods were chosen, despite being more expensive, as it would be easier to drill the holes into the square pieces versus another shape or material. The cost, however, was only $56.98 for a rod with dimensions of 2.54 cm by 3.175 cm by 152.4 cm and provided the sufficient strength required. The journals connecting the webs for the crankshaft did not need to be drilled vertically and could therefore be cylindrical. For a 61 cm rod with a diameter of 1.27 cm, it would be cost $11.28.

The driveshaft, a steel, hexagonal shaft, was recycled from the previous MQP and was durable, machinable, and mostly resistant to corrosion. This shaft held up to the forces that exist

while it converted the rocking motion to a rotating motion. The fin was constructed of fabric-reinforced neoprene as it needed to be flexible yet durable as it moved with the water. This type of neoprene has a tensile strength of 1500 psi within an operating temperature range of -30 to 200 degrees Fahrenheit. For a sheet dimensioned 0.16 by 30.5 by 122 cm, it costed about $75 (McMaster, 2015).

## 3.3.2 Finite Element Analysis of Components

In order to determine the materials used to create the crankshaft and the fin, CAD models were subjected to finite element analysis (FEA) using Ansys Multiphysics software. Ansys is a powerful physics simulation program that allows direct analysis of CAD files with a number of different modules. Critical for this project, Ansys contains both fluid dynamics and structural analysis modules which can feed results into each other. Using the fluid dynamics module, the forces on the fin model were found and then relayed to the structural analysis module. The water was defined as flowing at 2.0 m/s, the maximum flow velocity we can expect to achieve in our testing. This was coupled with varying the material composition of the masts. This system is depicted below in Figure 18. Materials considered were required to be corrosive resistant in chlorinated water, such as brass, certain stainless steels, aluminum and several polymers.

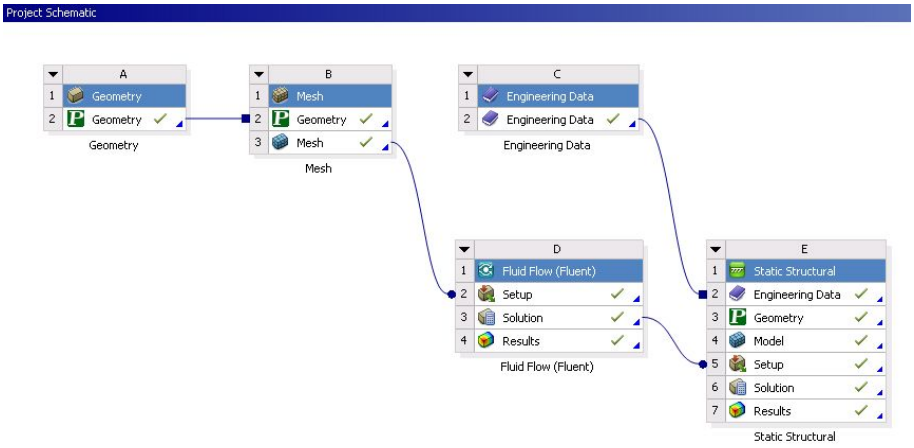


*Figure 18: Ansys Simulation Setup*

Ultimately, this analysis led to the decision to choose stainless steel to create the rod. It was chosen because it will not plastically deform or suffer brittle failure at the expected loads, while also being the cheap to procure and the most stable in chlorinated water. A table of the materials, cost and whether it passed or failed the test is below. For the tests, a model of the fin was created and imported into Ansys. Using a computational fluid dynamic modeler, the forces that the mast experience were modeled. This information was then used in a structural analysis of the fin, which was used to determine which materials would withstand the projected forces. More detailed results of the FEA programs can be found in Appendix 2.

*Table 2. Mast Material Analysis*

| Material | Cost per 30.5 cm length (25.4 cm diameter) | Pass/Fail? |
|---|---|---|
| 304 Stainless Steel | $2.42 | Pass |
| 464 Naval Brass | $6.19 | Pass |
| 6/6 Nylon | $0.45 | Fail |
| 6061 T6 Aluminum | $2.00 | Pass |
| Polycarbonate | $1.22 | Fail |

The crankshaft was also designed using FEA. The major consideration in designing the crankshaft was the material selected. The initial crankshaft design called for the use of 6061 aluminum components. However, aluminum is both more expensive at $\$0.0418/cm^3$ compared to $\$0.0277/cm^3$ for acrylic. Aluminum also requires more tooling and longer cycle times than acrylic. Therefore, FEA was used to determine if acrylic was strong enough to withstand the forces that would be experienced during operation of the device. We applied a load of 6 N on each crank journal, well in excess of the 3 N*m total torque measured in the previous experiments, and placed bearings each support journal. The loading can be seen in Figure 12. These calculations demonstrated that the stresses experience would remain within the plastic deformation range. The tensile strength of acrylic is 69 MPa at yield, and the compressive

strength is 124 MPa yield, both far surpassing the calculated stresses on the crankshaft. Acrylic has a shear strength of about 62 MPa, which is more than two thousand times the shear stress experienced by the shaft, as demonstrated in Figure 19 and Figure 20. While the model assumes that the loads will be applied directly in line with the journals, this is unlikely to occur in testing. However, the acrylic so vastly outperformed the tests, it is reasonable to believe that it should be able to survive any misaligned loading.

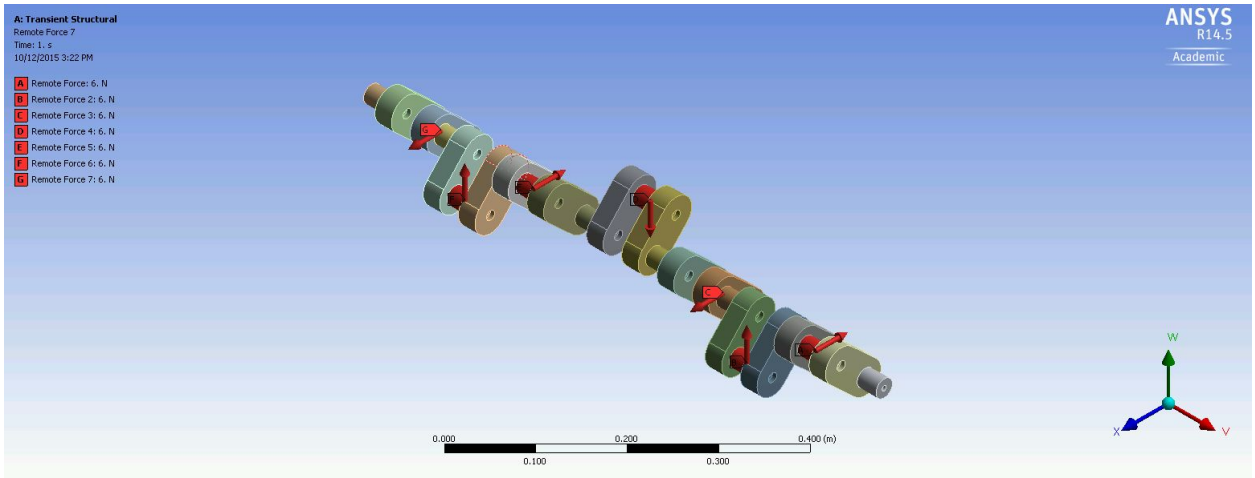


*Figure 19: Crankshaft Loading*

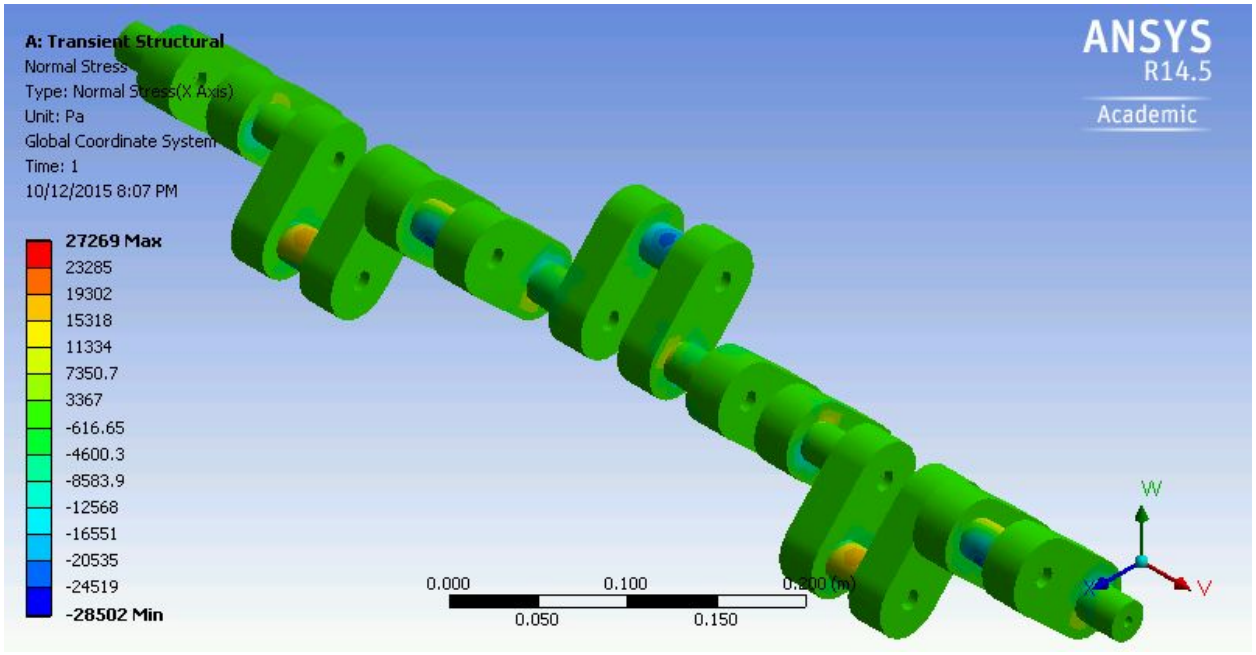


*Figure 20. Normal Stress Calculated by Ansys*

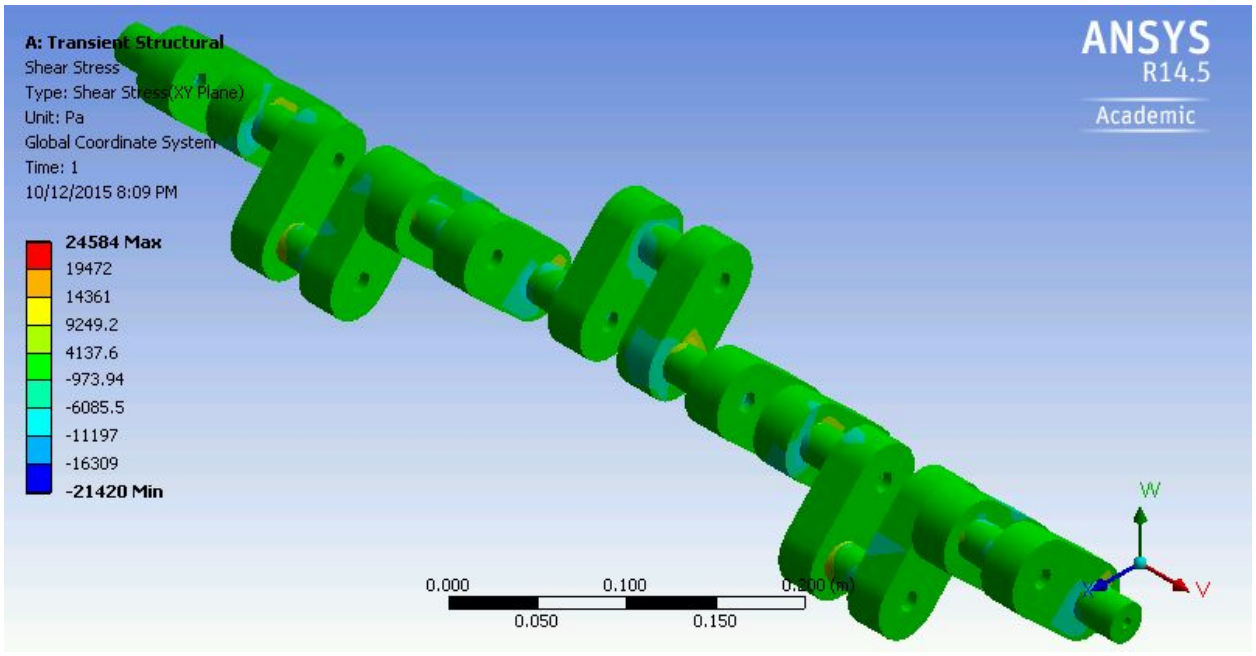


*Figure 21: Shear Stress Calculated by Ansys*

## 3.4 Manufacturing

All components were designed to be manufactured using local capabilities, such as a CNC mill and a two-dimensional laser cutter in Washburn Shops. These resources allow us to machine a wide variety of part sizes and materials with high tolerances and relatively short cycle times.

### 3.4.1 Materials

The materials that the design will use include acrylic, which is predominantly used in the camshaft and crankshaft assemblies, neoprene sheets, extruded 80-20 aluminum, and brass rods. There are also several driveshafts, bearings, fasteners and supports used, many of which were off-the-shelf products to reduce manufacturing demands. Materials were generally chosen with attention to machinability and stability in water to avoid corrosion.

The camshaft assembly is built with acrylic cams resting on stainless steel ball bearings and mounted on a steel driveshaft. The crankshaft is built from acrylic components bonded with glue and bolted together. Due to the weight of the crankshaft, the shaft is supported by several bearings mounted to 3D printed supports. The fin is built out of brass rods with neoprene sheets to catch the flow of water, with acrylic boning between sheets.

### 3.4.2 Production

Generic parts including the bearings, driveshafts, and fasteners were obtained off-the-shelf. The custom created parts were machined using a variety of tools, including vertical CNC mills a laser cutter, and a MakerBot 3D printer.

#### 3.4.2.1 Rocker Production

Rockers were designed and printed to mount directly to the fin masts. All seven rockers were printed out of ABS plastic using a 3D printer. The rockers were then mounted onto a ¼ steel shaft and locked in place by securing a threaded nut with Locktite on each side of all of them. The camshaft attaches directly to the rockers with bolts and is prevented from moving laterally by PTFE washers. The crankshaft is attached by aluminum rods that are mounted to 3D printed ABS blocks, which are bolted into the rockers using the same scheme and hardware as the crankshaft.

#### 3.4.2.2 Camshaft Production

The camshaft was machined using a VLS 4.60 Laser Cutter. This allowed parts to be directly converted from SolidWorks drawings to machine instructions, facilitating easy production of many identical components. Due to the size limitations of the laser cutter, acrylic pieces needed to be created in multiple parts and bonded together. Typical acrylic glue was used to weld the pieces together, achieving a bond strength around 14 MPa, far exceeding the calculated loads.

During machining tolerances and the need for high tolerance pieces, several iterations of the camshaft were cut and tested until a design was achieved that both securely held the ball bearings in place and allowed for the free rotation of the cams. A total of 13 iterations were tested, the changes made between each iteration was changing the inner and outer circles of the cam design by hundredths of an inch. Notably, the middle cam had a slightly large cut to create a channel in which the ball bearings could rest.

Once all the acrylic was cut, the cams were assembled. Each cam contained six acrylic pieces, as well as twenty-seven ¼ inch diameter ball bearings. The six acrylic pieces can be seen in an exploded view in Figure 22 below. The cams were assembled by first aligning and bonding together one of the out cam pieces with the center piece, making sure that the holes for the shaft

were aligned. Next, the balls were placed into the ring made by the inner circles and outer cam piece. Lastly, the second outer piece was aligned and bonded. The cams were then held in place with a clamp to allow to bonding agent to properly bond the pieces together. This method was chosen over notching the acrylic to fit the bearings in because it was less likely to damage the acrylic and it was less likely the bearings would pop out when pressure was applied.

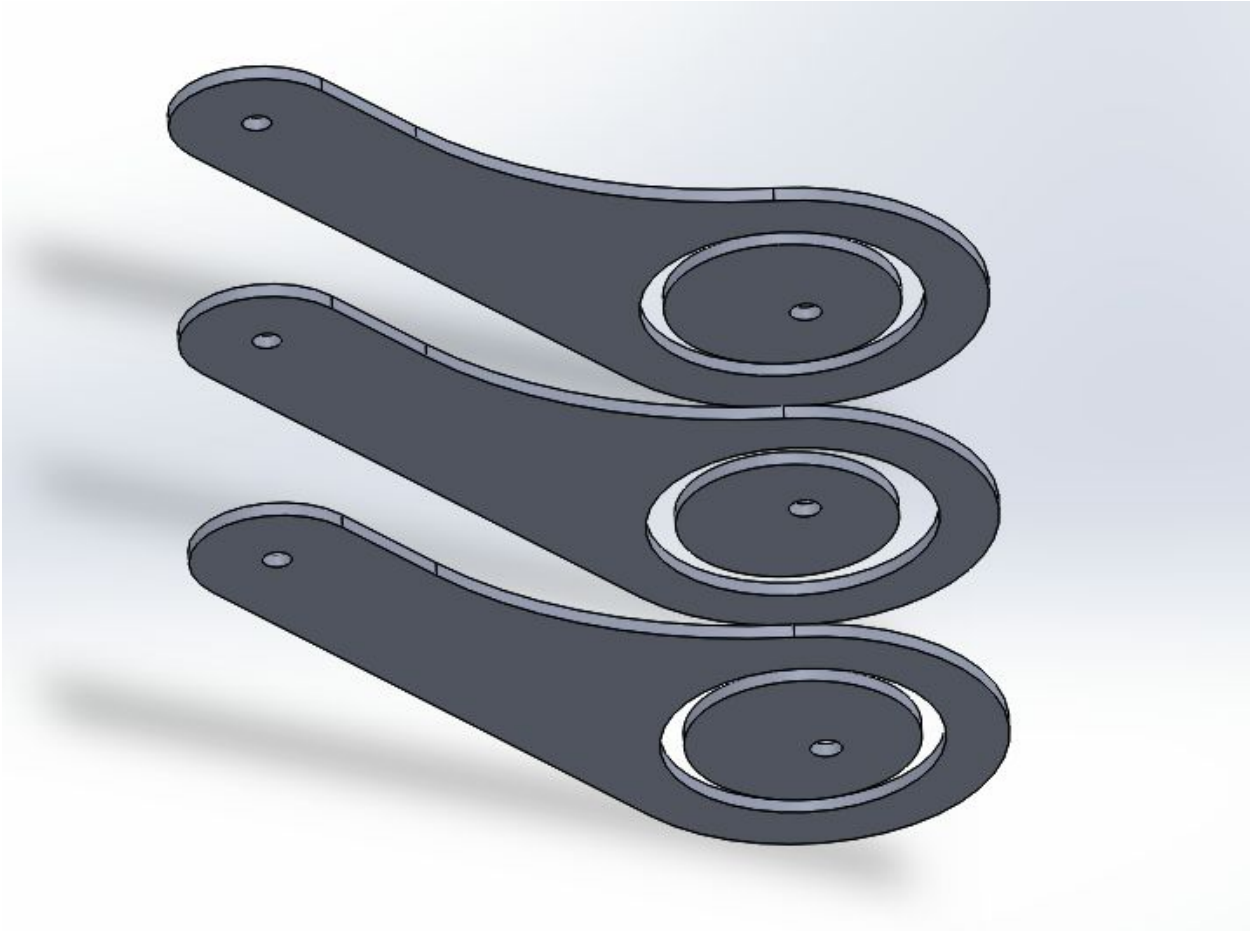

*Figure 22: Exploded View of One Cam Assembly*

### 3.4.2.3 Crankshaft Production

The acrylic components of the crankshaft were machined using a bandsaw, while CNC mills were used to drill all necessary holes. The crankshaft was machined and attached in pieces to ease manufacturing and lower costs. The shaft was created using an acrylic rectangular rod and a round rod. The pieces were cut to length using the bandsaw then both bolted and bonded together to ensure the journals and webs would stay at the proper angle relative to each other. The round rod was used for the webs and are connected to the rockers using bearings with 3D printed sleeves that hold an aluminum rod. Another 3D printed piece was printed to hold the other end other the aluminum rod to the rocker. A stainless steel driveshaft was purchased to avoid a high tolerance machining operation, as well as the providing the benefit of being completely stainless with no risk of damaging the finish during manufacturing. The drive shaft was connected at the end of the crankshaft and is connected to the motor through a lovejoy coupling.

### 3.4.2.4 Frame Production

The test frame is made of 80-20 aluminum. The shafts are supported by off-the-shelf bearings mounted in sheets of laser cut acrylic. This is necessary due to the weight of the crankshaft and the deflection of the rocker shaft. The camshaft and crankshaft use an interchangeable mounting scheme so that they can quickly and easily be switched to facilitate testing. The fins were originally permanently mounted to rockers, which had interchangeable mounting scheme so that they could easily be mounted to either the camshaft or the crankshaft. It was important to minimize changes between the different device configurations, to allow accurate direct comparisons of device performance between the cam and crank shafts.

## 3.5 Testing

### 3.5.1 Testing Environment

To evaluate both designs using the crankshaft and the camshaft, adequate testing space was needed. The swimming pool located at WPI's Sports and Recreation Center provided sufficient space to test the designs. By using the school's equipment and facilities, special consideration was required to ensure damage will be prevented. For this, testing rigs have been designed and constructed for use in the space. The previous testing rig design was used and reconstructed as no problems had occurred when in operation. The rig consisted of a metal frame supported by a set of pontoons allowing the neoprene fin to be the only element of the design exposed to the water. Because the fin only occupies a fraction of the pool volume, it is assumed to be an infinite body of water. The mechanism attached to the rig was then pulled through the water using rope to simulate a flow on the fin. This design considered the weight of the assembly, portability from one location to another, and ease of assembly.

### 3.5.2 Testing Procedure

A few different tests were planned in order to collect usable data that could be analyzed and determine the efficiency of the device built. First, the team wanted to test the neoprene fin in conjunction with the cam shaft, in order to test efficiency of the single sheet neoprene fin as compared to the hybrid fin designed by the previous MQP. This would have isolated the variable of the fin and given a better understanding of which modified aspect of the design led to better efficiency. However, due to setbacks that did not allow for the installation of electronic components (which are outlined later on in this paper), not all of the planned testing was able to be executed. After setting up dockside electronic equipment, the nacelle would then have been attached to the frame and the device will be mounted onto the pontoon supports and the sensory inputs would have been initialized. The mounted system, attached to the wench and guide ropes, was placed in the water in alignment with the guiding lanes in use. The data collection then

would have begun and the motor started. The device was pulled across the pool, with assistance from the guide ropes, first at a speed of 1 m/s, and the appropriate data values collected. This test was then be repeated at a speed of 2 m/s, in order to see possible changes in efficiency at different flow rates. When the device reached the end of the pool lane, the motor would have been turned off. This ended the data collection for this individual test and the device was removed from the testing environment.

After the device has been tested with the camshaft to completion, the team then replaced the camshaft with the designed crankshaft and was tested following the same procedure as above, testing the same variables in order to effectively compare it to the data obtained from the previous testing iteration.

### 3.5.3 Testing Variables

For the performance of the device to be properly evaluated, several variables of the device and testing environment were to be manipulated. However, in order to facilitate the comparison of this design with the previous design many of the testing variables were kept the same as they were for the previous design. Therefore the independent variables and dependent variables were fin configuration, fin height, flow velocity, torque, shaft type, rotations per minute (RPM), and power output.

For this experiment both the fin configuration and fin height were kept the same throughout testing. This constant was chosen in order to compare the design of this project with the fin design of the previous MQP. This choice was also made due to time constraints as it was infeasible to test both a cam and a crank shaft designs for more than one fin model in the time period given.

The flow velocity was determined to be an independent variable. By varying the flow velocity the device can be tested under different flow conditions and an ideal flow velocity could be determined based on a power curve created over the range of flow velocities. In order to test

for flow velocity, a motorized winch was used to accurately pull the rig at a constant speed that was changed after each test.

The shaft type was varied between a cam shaft and a crankshaft. The shafts were interchangeable and half the tests were performed using the cam shaft, while the other half of the tests were performed using the crankshaft. These two designs were interchanged in order to test the theory that a crankshaft is better suited for this device. The power outputs and efficiencies of both shafts over the range of flow velocities were plotted and compared in order to determine which shaft is a better design choice. The torque was varied using a mechanical device. The torque was varied to represent different loads that could be attached to the shaft in order to determine the range of the device.

One dependent variable of these tests was to be the output from the motor. The power output is most indicative of the performance of this device and was to be measured using the data produced by an electric motor.

# 4. Conclusions and Recommendations for Continuation of Project

When building the device, the team ran into several setbacks. The first was the feasibility of manufacturing a crankshaft on WPI's campus. It quickly became apparent that manufacturing a crankshaft out of acrylic would not be as successful an endeavor as they had hoped. While, eventually, the group was successful in assembling a crankshaft, they learned that the necessary tolerancing was not feasible to manufacture, and this led to many failed attempts at assembly. Not only this, but industrial strength acrylic glue that was hoped to partially adhere the journals to the webs of the shaft (in combination with bolts through each segment) did not hold up well enough to the forces necessary to turn the shaft. The strength of the adhesive was adequate, however only after a setting time that did not line up well with the timeline of this project. Not only this, but there was significant bowing of the shaft when fully assembled due to the weight of

the acrylic added for strength. Acrylic is more brittle than steel, and therefore thicker pieces of acrylic were used for the journals and webs in order to increase the strength of the shaft. This was unsuccessful in that the adhesive could not handle the extra weight of the acrylic and the shaft had a tendency to bow. Because of all of these factors, it is advised in the future that a crankshaft should not be manufactured on campus for a similar project unless the project team has the budget and skills necessary to weld steel for a more successful product. Otherwise, a custom-ordered crankshaft is a better, though less cost-efficient, option.

Another short sighting of this project was the weight of the fin. While the mathematics showed that a fin made out of a single sheet of neoprene was the best option in terms of power transferred from the water, the design of the fin ended up having too much weight to turn the shafts based on the force applied when dragged through the water. This weight caused the shaft to bind up where bowing occurred and prevented rotation. Most of this can be attributed to the fact that the team used two sheets of ⅛" neoprene adhered together to comprise the fin. After preliminary testing of the fin failed, a weight test was administered, where they removed the fin, and applied weight to the rods until the shaft refused to move. The maximum weight that would allow the shaft to rotate was 250 g per rod, which for seven rods would result in a total fin weight of 1.7 kg. This is the maximum weight for the fin that would be successful in translating power through the shafts. For continuation of the project, the recommendation would be either to find a way to make the fin out of a single sheet of ⅛" thick or thinner neoprene, or to find a material that is even lighter that could withstand the forces from the water. One suggestion would be to research a synthetic fabric, such as waterproof canvas, or another thin, water-impermeable fabric. This would achieve the desired functionality while still being light enough to require less force to turn the shaft.

The final recommendation, in order to achieve a more efficient camshaft, is to increase the size of the metal frame. Due to size constraints, the team was unable to use their original cam design with a smaller inner circle radius and a longer neck, which was designed to eliminate the

dwell that was present in the previous team's design. This dwell significantly increased the force necessary to turn the shaft, lowering the efficiency of the product as a whole and limiting the power that was produced. A larger shaft would allow for a longer cam, which increases the probability of eliminating the dwell altogether.

In conclusion, the future of this project highly depends on the design choices of future project teams. Implementing these recommendations and learning from this year's project team's errors are essential to the success of future design iterations. Because of the setbacks that the team faced, palpable, quantitative results were not collected, and most of the time spent was used trying to modify the design in order to produce a working prototype. Future teams should take note of what did not work for this project, and move forward with their own hypothesis of what may be more efficient and manufacturable.

# References

Blevins, E. L., & Lauder, G. V. (2012). *Rajiform locomotion: three-dimensional kinematics of the pectoral fin surface during swimming in the freshwater stingray Potamotrygon orbignyi*. Journal of Experimental Biology.

Boileau, R., Fan, L., & Moore, T. (2002). *Mechanization of Rajiform Swimming Motion.* The making of Robo Ray.

Choucri, N. (2012). *Renewable Energy Technologies: Cost Analysis Series,* Hydropower. Volume 1: Power Sector. Energy and Development: Fossil Fuels in Developing Countries. Energy for Survival and Development(57).

Costanzo, I., Kelsey, A., Ogren, F., Wians, D. (2015) *Design of a Novel Concept for Harnessing Tidal Stream Power*. Major Qualifying Project, Worcester Polytechnic Institute.

DTI. (2002) Engineering Business: *Research and Development of a 150kw Tidal Stream Generator - Phase 1*. Retrieved from http://www.dti.gov.uk/renewables/publications/pdfs/T00211.pdf

DTI. (2003) Engineering Business: *Research and Development of a 150kw Tidal Stream Generator - Phase 2*. Retrieved from http://www.dti.gov.uk/renewables/publications/pdfs/T00211.pdf

DTI. (2005) Engineering Business: *Stingray Tidal Stream Energy Device Phase 3*. Retrieved from http://www.dti.gov.uk/renewables/publications/pdfs/T00211.pdf

*Environmental Impacts of Hydroelectric Power.* (2015). Union of Concerned Scientists.

Epstein, M., Colgate, J. E., & MacIver, M. A. (2006). *Generating thrust with a biologically-inspired robotic ribbon fin*. 2412-2417.

Friedel, Robert. (2007). A Culture of Improvement: Technology and the Western Millennium

Friction and Coefficients of Friction. (2016). Retrieved from http://www.engineeringtoolbox.com/friction-coefficients-d_778.html

Herrel, A., Choi, H., De Schepper, N., Aerts, P., & Adriaens, D. (2011). *Kinematics of swimming in two burrowing anguilliform fishes*. Zoology, 114(2), 78-84.

*How Geothermal Energy Works.* (2015). Union of Concerned Scientists.

*How Solar Energy Works.* (2015). Union of Concerned Scientists.

International Energy Agency, & Electronic Journals Library. (1998). Key world energy statistics from the IEA. *Key World Energy Statistics from the IEA*

Key World Energy Statistics. (2014). Retrieved: http://www.iea.org/publications/freepublications/publication/KeyWorld2014.pdf

Lauder, G. V., & Drucker, E. G. (2004). *Morphology and experimental hydrodynamics of fish fin control surfaces*. IEEE Journal of Oceanic Engineering, 29(3), 556-571.

McMaster-Carr. (2015). Retrieved from http://www.mcmaster.com/

Murray, Peter. (2012) *First Offshore Turbine For U.S. Begins Feeding Power To Maine's Grid.* Retrieved from http://singularityhub.com/2012/11/01/first-offshore-turbine-for-u-s-begins-feeding-power-to-maines-grid/

Navigant Consulting, Inc. (2009). *Job Creation Opportunities in Hydropower*. Retrieved from http://www.hydro.org/wp-content/uploads/2010/12/NHA_JobsStudy_FinalReport.pdf

NREL (2015). Levelized Cost of Energy Calculator. Retrieved: http://www.nrel.gov/analysis/tech_lcoe.html

Niu, X., Xu, J., Ren, Q., & Wang, Q. (2014). *Locomotion learning for an anguilliform robotic fish using central pattern generator approach.* IEEE Transactions on Industrial Electronics, 61(9), 4780-4787.

Norton, R. L. (2012). *Design of machinery: An introduction to the synthesis and analysis of mechanisms and machines* (5th ed.). New York: McGraw-Hill.

Prono, L. (2012). *Alliance to Save Energy*. In S. G. Philander (Ed.), Encyclopedia of Global Warming & Climate Change (2nd ed., Vol. 1, pp. 36-38). Thousand Oaks, CA.

Rosenberger, L. J. (2001). *Pectoral fin locomotion in batoid fishes: undulation versus oscillation*. Journal of Experimental Biology.

Singh, Timon. (2012) *Maine Launches the First Commercial Tidal Power Project in the US!.* Retrieved from http://inhabitat.com/maine-launches-the-first-commercial-tidal-power-project-in-the-us/

Thompson, Ross. (2009). Structures of Change in the Mechanical Age: Technological Invention in the United States

*Types of Renewable Energy: A Cost Comparison.* (2015). Green Electricity Guide

U. N. D.P. (2000). World Energy Assessment - Energy and the Challenge of Sustainability. Retrieved from http://www.undp.org/content/dam/aplaws/publication/en/publications/environment-energy/www-ee-library/sustainable-energy/world-energy-assessment-energy-and-the-challenge-of-sustainability/World%20Energy%20Assessment-2000.pdf

U.S. Energy Information Administration (EIA). (2015). *Future world energy demand driven by trends in developing countries*. Today in Energy. Retrieved from http://www.eia.gov/todayinenergy/detail.cfm?id=14011

US EPA. (2015). *Energy and the Environment.*

US EPA. (2015). *Future Climate Change.*

US EPA. (2015). U.S. Greenhouse Gas Inventory Report.

Wikander, Örjan. (1999). *Handbook of Ancient Water Technology*

William S. Vorus Brandon M. Taravella. (2011). *Anguilliform fish propulsion of highest hydrodynamic efficiency*. Journal of Marine Science and Application, 10(2), 163-174.

Wind and Solar Energy. (2015). Retrieved from http://www.cleanlineenergy.com/technology/wind-and-solar

World Nuclear Association (2011). Comparison of Lifecycle Greenhouse Gas Emissions of Various Electricity Generation Sources. Retrieved from http://www.world-nuclear.org/uploadedFiles/org/WNA/Publications/Working_Group_Reports/comparison_of_lifecycle.pdf

Woody, T. (2015). *Here's Why Developing Countries Will Consume 65% of the World's Energy by 2040.*

# Appendices

## Appendix A: Fin Dimensions

$len := 30$

$x := 0, 0.01 .. len$

$n := 5$

$$\lambda := 360 \cdot \frac{\left(\frac{30}{7}\right)}{15 \cdot n}$$

$\lambda = 20.571$

$rtip := 13$

$rbase := 1$

$$\theta max := 45 \frac{\pi}{180}$$

$$form(x) := \theta max \cdot \sin\left(2\pi \frac{x}{\lambda}\right)$$

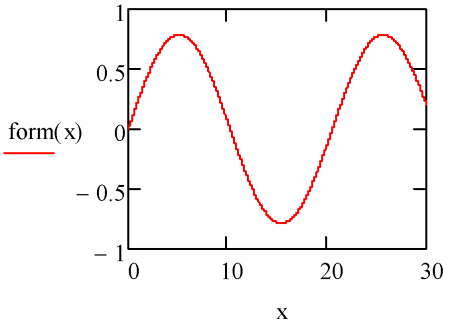


$$edgeL(r) := \int_0^{len} \sqrt{1 + \left[\frac{d}{dl}((form(l) \cdot r))\right]^2}\, dl$$

$$Ltip := edgeL(rtip) = 67.937$$

$$Lbase := edgeL(rbase) = 30.415$$

$$r1 := Lbase \cdot \frac{(rtip - rbase)}{(Ltip - Lbase)} = 9.727$$

$$r2 := rtip - rbase + r1 = 21.727$$

$$\theta := \frac{Lbase}{r1} = 3.127$$

$$\theta := \frac{Ltip}{r2} = 3.127$$

$$3.127 \cdot \frac{180}{\pi} = 179.164$$

# Appendix B: FEA Program Results

Program Set Up:

The fin and mast assembly was first created in SolidWorks. All surfaces were then joined to create a single solid body. This was then exported as a parasolid file (.x_t file extension) to be used in Ansys. A second identical copy was made, with the exception of a large, thin disk placed in front of the fin to be used as a flow generation source. This was also exported as a parasolid. The flow was set to 2 m/s, the maximum velocity expected during testing. The fin and disk were imported as a geometry (A), then meshed using a CFD mesh optimized for Fluent (B), which was then imported into a Fluent CFD solver (D). The materials for the fin and the various mast types were assigned in an engineering data library (C). The solution of the Fluent analysis was then imported into a structural analysis (D), which produced the stress estimates desired. An image of this schematic is below. Fluent was used to model the expected forces on the fin as it moved through the water. The boundary conditions were set to be a constant 2 m/s flow and generated from a source large enough to avoid potentially confounding results from boundary interactions with the fin. This result was fed into a structural analysis which then determined which materials would be outside of their operational range for our application.

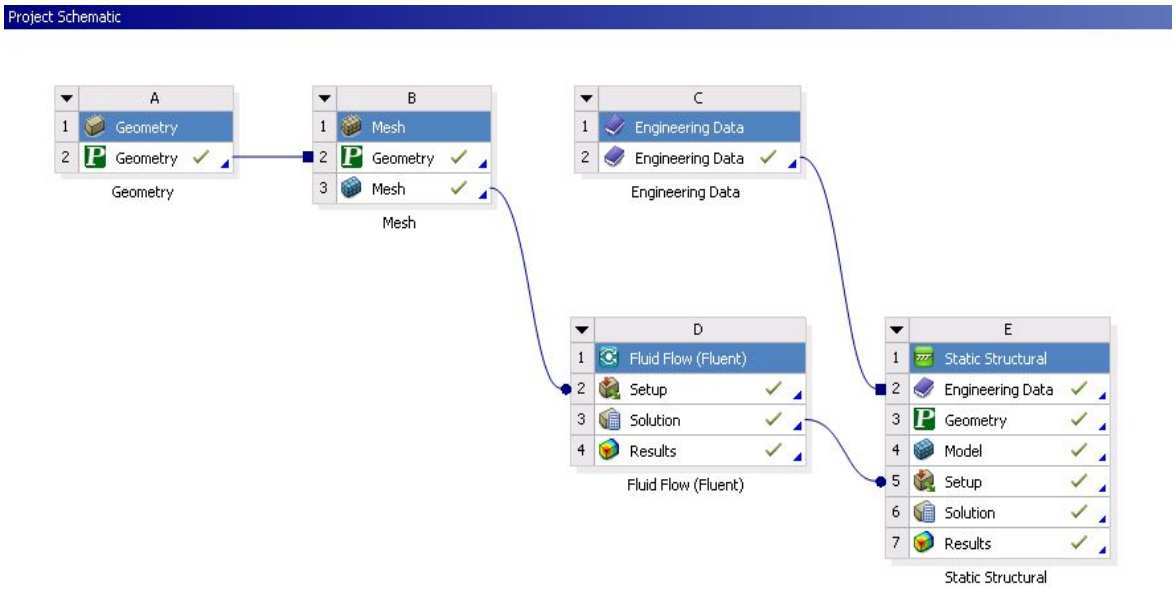


*Figure 17. Ansys Simulation Setup*

Results for different materials are pictured below.

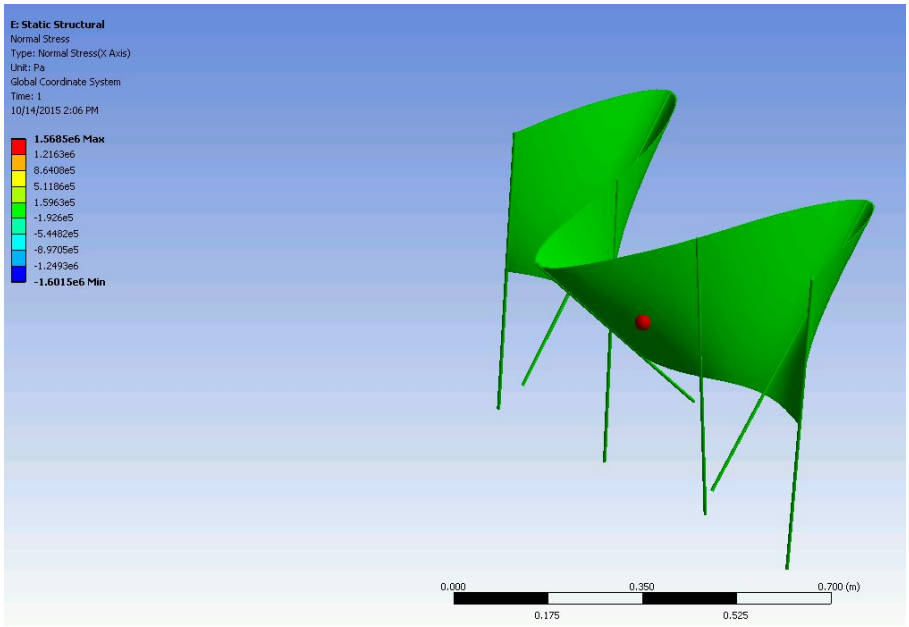


*Figure 18. Normal Stress on Aluminum Masts*

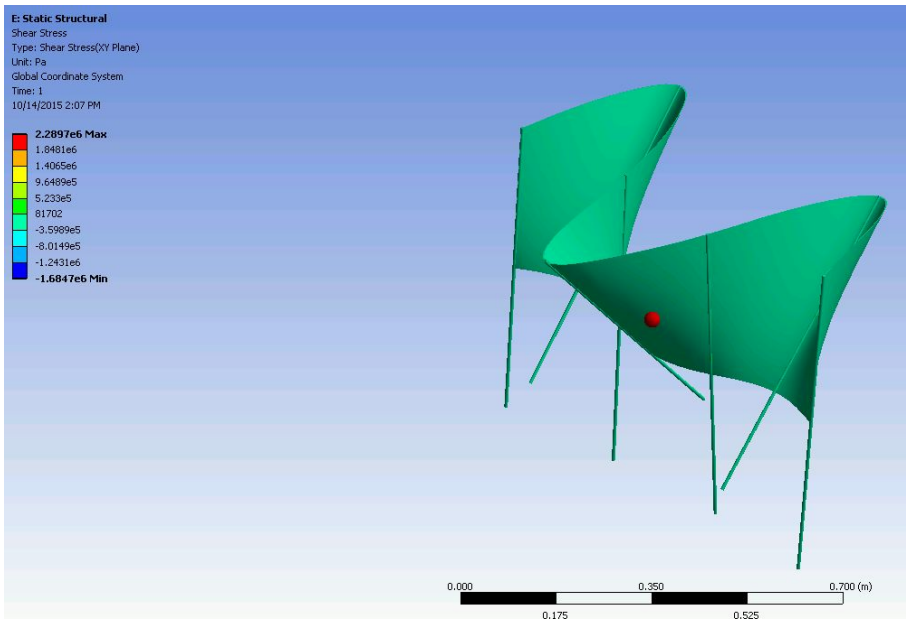


*Figure 19. Shear Stress on Aluminum Masts*

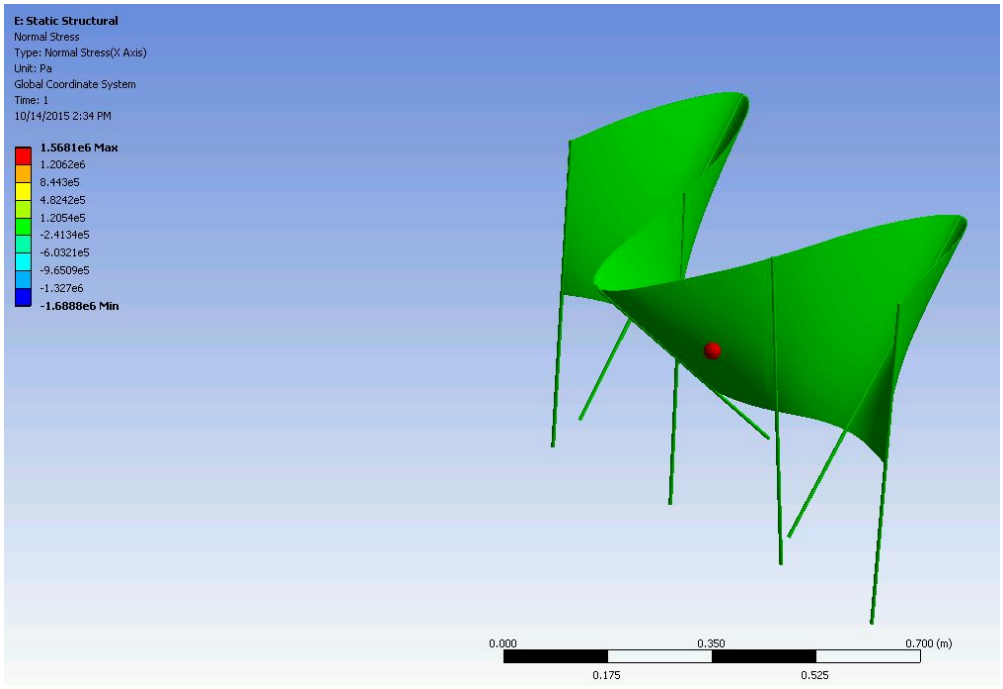


*Figure 20. Normal Stress on Brass Masts*

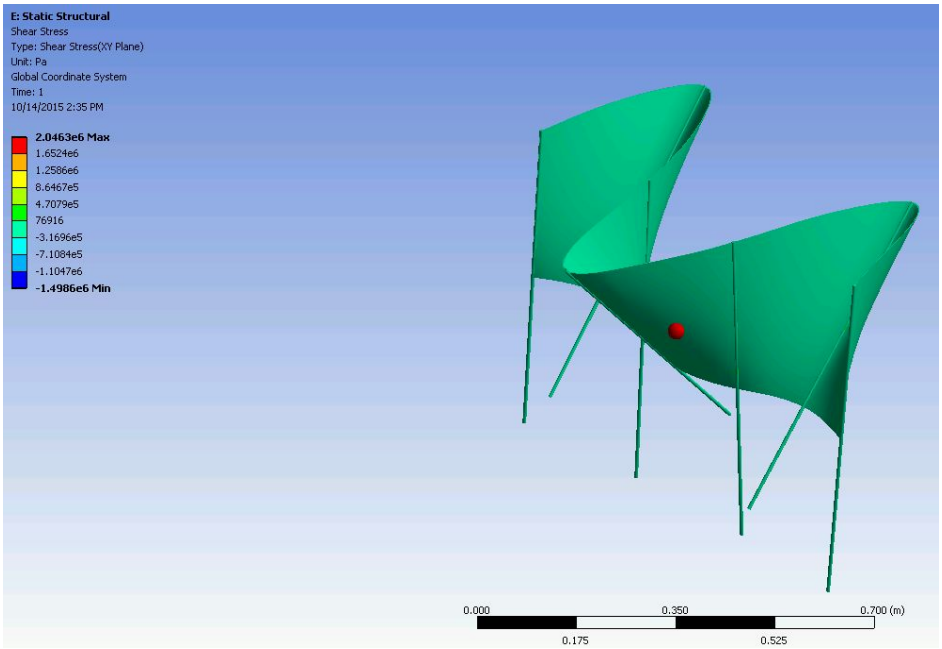


*Figure 21. Shear Stress on Brass Masts*

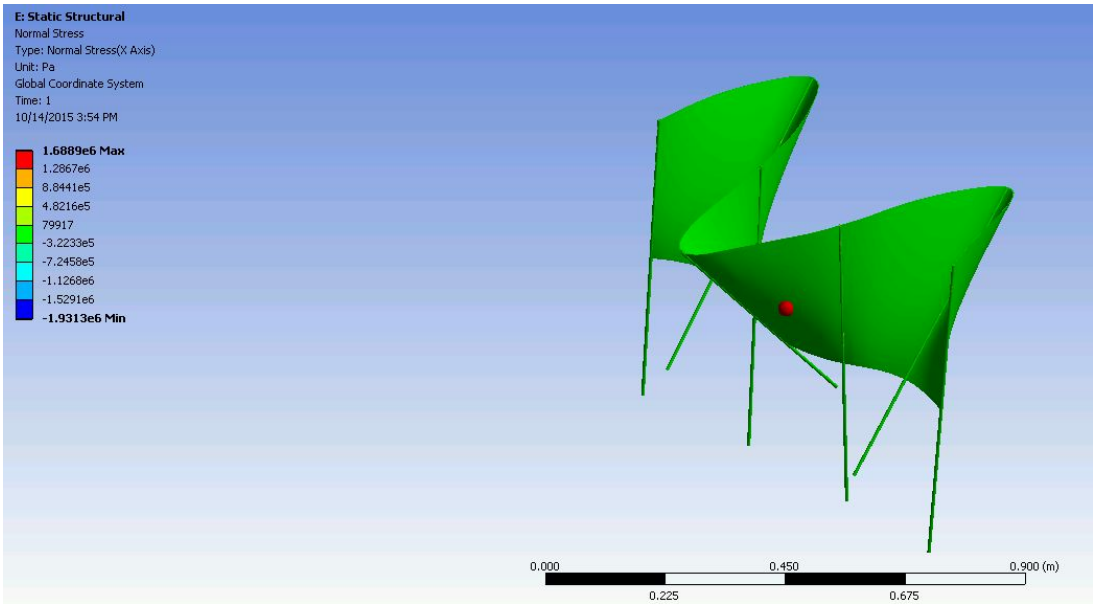


*Figure 22. Normal Stress on Stainless Steel Masts*

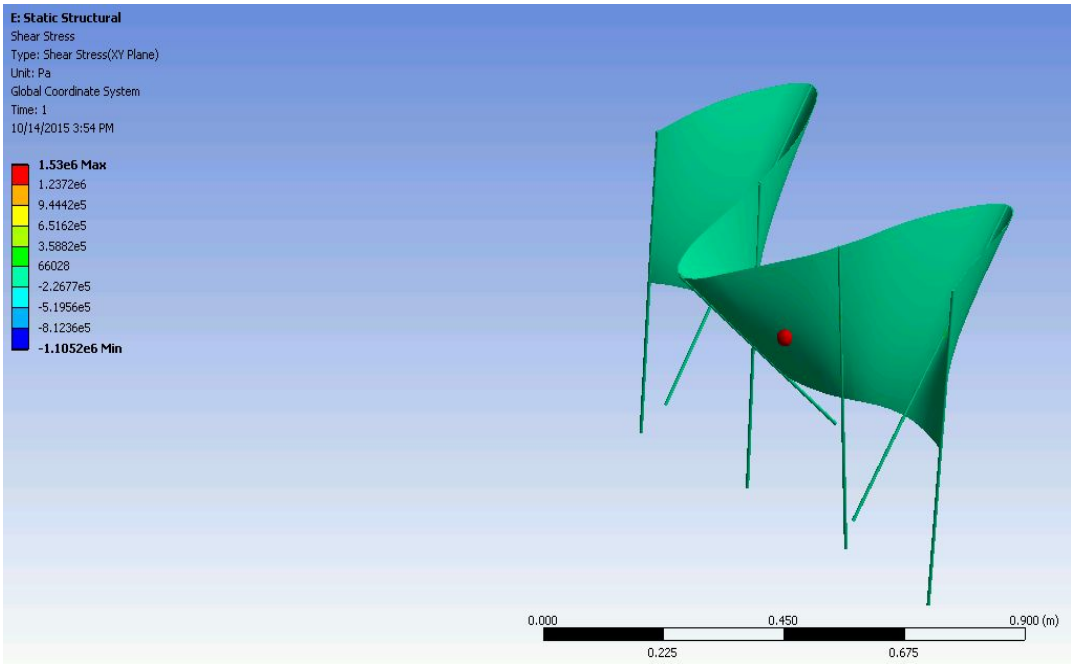


*Figure 23. Shear Stress on Stainless Steel Masts*

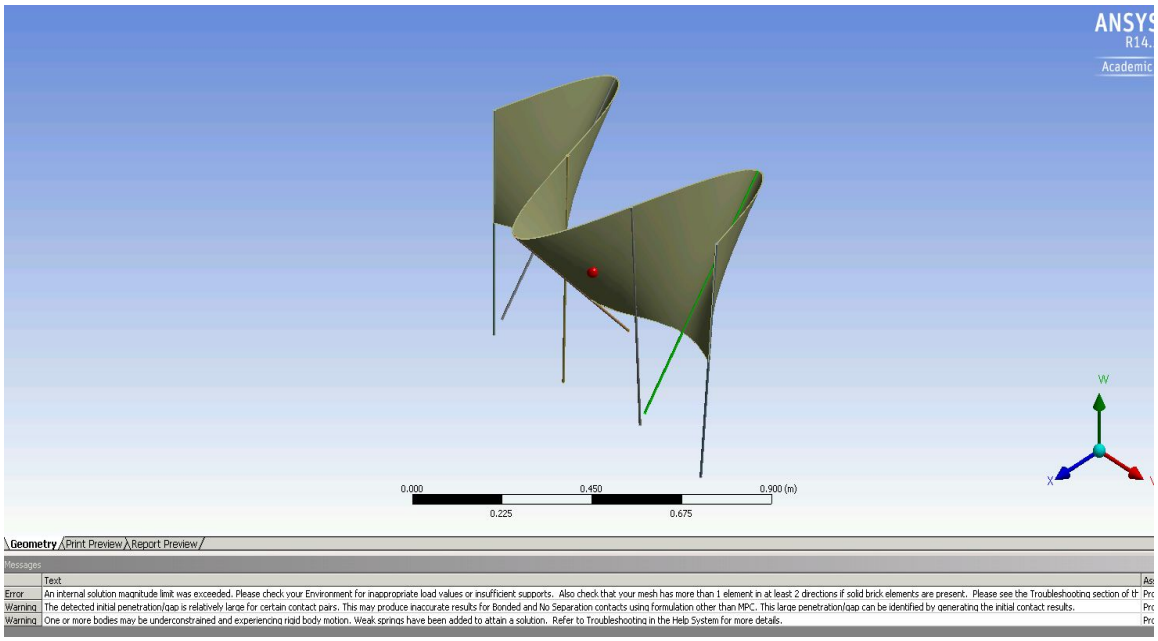


*Figure 24. Failed Nylon Masts*

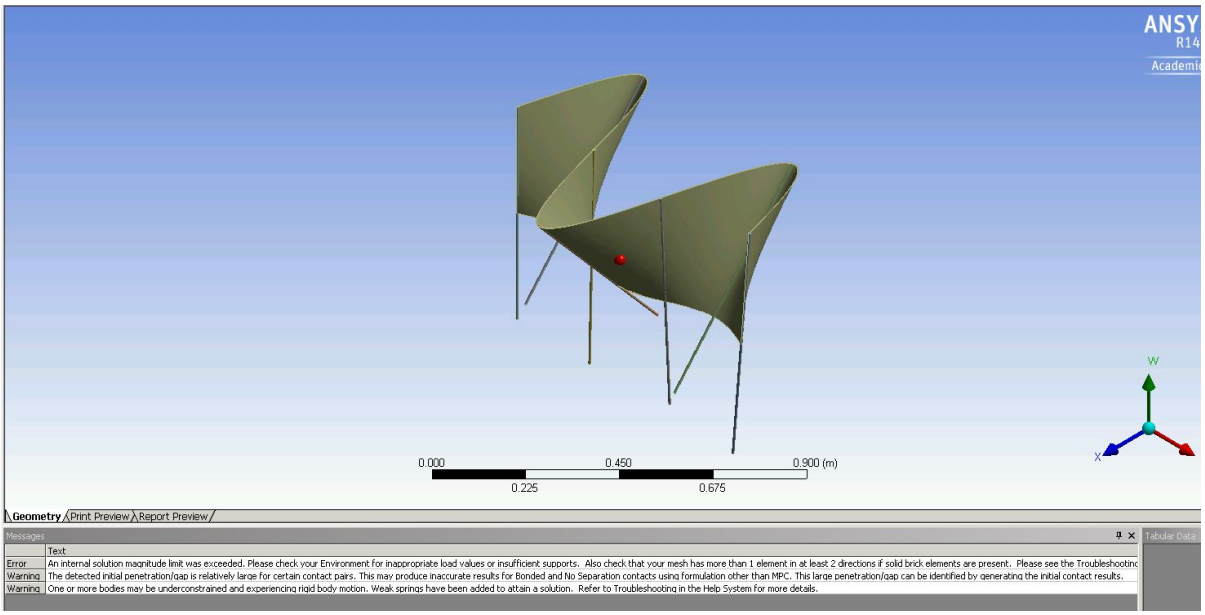


*Figure 25. Failed Polycarbonate Masts*